J. Fluid Mech. (1993), *vol.* 253, *pp.* 385–419

Vortex dynamics and the production of Reynolds stress

By PETER S. BERNARD[1], JAMES M. THOMAS[1] AND ROBERT A. HANDLER[2]

[1] Department of Mechanical Engineering, University of Maryland, College Park, MD 20742, USA
[2] Naval Research Laboratory, Washington, DC 20375, USA

(Received 4 August 1992 and in revised form 12 January 1993)

The physical mechanisms by which the Reynolds shear stress is produced from dynamically evolving vortical structures in the wall region of a direct numerical simulation of turbulent channel flow are explored. The complete set of quasi-streamwise vortices are systematically located and tracked through the flow by the locus of the points of intersection of their centres of rotation with the (y, z) numerical grid planes. This approach assures positive identification of vortices of widely differing strengths, including those whose amplitude changes significantly in time. The process of vortex regeneration, and the means by which vortices grow, distort and interact over time are noted. Ensembles of particle paths arriving on fixed planes in the flow are used to represent the physical processes of displacement and acceleration transport (Bernard & Handler 1990*a*) from which the Reynolds stress is produced. By interweaving the most dynamically significant of the particle paths with the evolving vortical structures, the dynamical role of the vortices in producing Reynolds stress is exposed. This is found to include ejections of low-speed fluid particles by convecting structures and the acceleration and deceleration of fluid particles in the cores of vortices. Sweep dominated Reynolds stress close to the wall appears to be a manifestation of the regeneration process by which new vortices are created in the flow.

1. Introduction

The central role of the Reynolds shear stress in the analysis and modelling of turbulent flows has stimulated attempts at finding a physical explanation for the transport inducing fluid motions associated with its definition as an average momentum flux. Spurred by recent results from direct numerical simulations, it has become increasingly clear that the underlying mechanisms of Reynolds stress production are inextricably linked to the dynamics of organized coherent vortical structures in the wall region. Current descriptions of this physical process, especially the dynamical aspects, remain incomplete, however, owing to gaps in understanding the characteristics of vortical structures in the high-Reynolds-stress producing region close to walls. A principal objective of the present work is to develop a sufficiently complete picture of the vortex evolution process in the near wall region, to be able to deduce how the Reynolds stress is produced as a natural consequence. The knowledge gained should improve the opportunities for devising better Reynolds stress models.

Among the first evidence linking vortices with the Reynolds stress was the $\overline{uv}$ quadrant decompositions of Wallace, Eckelmann & Brodkey (1972) in which the observed predominance of sweeps near the wall ($u > 0, v < 0$) and ejections further

from the wall ($u < 0, v > 0$), could plausibly be explained by the action of streamwise vortices. Here, (u, v) refer to the fluctuating velocity components in the streamwise and wall-normal directions, respectively, $\bar{U}$ is the mean velocity and $U = \bar{U} + u$. Evidence for the existence of quasi-streamwise vortices has accumulated from physical experiments including those of Kim, Kline & Reynolds (1971), Grass (1971), Smith & Schwartz (1983), Kasagi, Hirata & Nishino (1986) and others. Dynamical models of Reynolds stress production from quasi-streamwise vortices, usually in the form of counter-rotating pairs, have been formulated by Bakewell & Lumley (1967), Pearson & Abernathy (1984), Herzog (1986), Ersoy & Walker (1986), Jang, Benney & Gran (1986), Aubrey *et al.* (1988), Hanratty (1989), among others. More recently, Kline & Robinson (1989) and Robinson (1991*a*) have identified vortical structures through iso-surfaces of low pressure and noted their proximity to high-Reynolds-stress regions. Similar observations have been reported by Lyons, Hanratty & McLaughlin (1989) and Brooke & Hanratty (1993) based on their examination of end-on velocity vector plots. Jiminez & Moin (1991) have studied the dynamics of Reynolds stress production via a minimal flow simulation in which they discern a connection between Reynolds stress and vortices. Visualizations of fluid particle paths associated with Reynolds stress generation (Bernard & Handler 1990*b*; Handler *et al.* 1992) also provide considerable evidence to support a major role for vortical structures. Extensive discussion of the literature of coherent vortices has been provided recently by Robinson (1991*a*, *b*).

To achieve a sufficient understanding of the vortical structures to be able to relate their dynamics directly to Reynolds stress producing fluid particle motions, requires taking a closer and more detailed view of the flow than has been accomplished previously. In particular, it is necessary to locate the entire set of vortices in the near wall flow field, of all strengths and sizes, and to follow their motion in time as they are created, grow, distort and interact with neighbouring vortices. Our first task here is to develop a means of identifying and tracking vortices so that we will then be able to explore their relationship to the Reynolds stress. The identification scheme applied here appeals to the defining characteristic of vortices, namely, their rotational motion. The structures are categorized by the locus of their points of intersection with the spanwise grid planes of the simulation. As the physical vortices convect through the numerical mesh, their movements are followed through the motions of their central axes. The emphasis of this study is on vortices located within the inner part of the boundary layer, namely, from the wall outward to approximately $y^+ = 100$, a region encompassing the most active zone in so far as the production of Reynolds stress is concerned.

Early physical conceptions of the Reynolds stress (Hinze 1975) assume that it is a primarily diffusive phenomenon accountable for via a generalization of molecular transport models. Though this physical conception is not in contradiction with the imagined actions of vortices, it is poorly situated to take into account such questions as the size of the diffusive lengthscale in comparison to the scale of mean field variation, the notion of mixing and the potentially non-trivial role of fluid particle accelerations in generating Reynolds stress. As a consequence, simple diffusive models cannot account for the Reynolds stress in many anomalous flows where transport can be non-gradient, such as in a transpired or rotating channel, wall jet, and so on.

A recent work (Bernard & Handler 1990*a*, hereinafter referred to as BH) has formally addressed the question of the physics associated with Reynolds stress production by using a Lagrangian analysis of ensembles of fluid particle paths. Among the significant findings to emerge from this study is the notion of the mixing time, say

τ_m, as the time over which the Reynolds stress correlation is produced by specific events transpiring in the fluid. More precisely, if we consider an ensemble of fluid particles having the common property of arriving at a point a after travelling over the time interval τ, and denote the random initial points of the fluid particles by b, then, while $\overline{u_a v_a} = \overline{uv} \neq 0$, nonetheless, $\overline{u_b v_a} = 0$ if τ is sufficiently large. In other words, physical events occurring in the flow cause the velocity component u to develop its correlation with v_a over the time interval τ. τ_m may be taken as the smallest time at which $\overline{u_b v_a}$ is zero.

As shown in detail in BH, mechanisms entailing the displacement and acceleration of fluid particles underlie the u, v correlation. The displacement effect originates in the association of v_a with that part of u_a generated by the change in the mean field between positions b and a. This is the classic diffusive argument without the assumption that it is acceptably modelled through a gradient law. Indeed, BH showed that the latter possibility is far from the case. The second source of correlation lies in specialized accelerations coupling changes in U over the mixing time with v_a. Interestingly enough, it has recently been shown (Handler *et al.* 1992) that this is almost entirely a viscous effect for $y^+ \leqslant 40$, pressure forces becoming most significant only at $y^+ > 40$. To go beyond the physical description of Reynolds stress production attained in BH requires finding the source of the Reynolds-stress-producing fluid particle motions in the evolving vortical structures.

The next several sections describe our vortex identification scheme and the nature of the vortical field it reveals. The remainder of the work is concerned with integrating the dynamics of the particle paths into the life cycle of the vortical structures as a next step in understanding the physics of Reynolds stress.

2. Vortex identification

Apart from whatever mathematical ambiguities there may be in defining a vortex in wall-bounded flow (Blackwelder, Panton & Wallace 1989), our criterion for vortex detection is to be able to find each and every structure that has the appearance of a vortex. The formidable size of the simulation databases has previously favoured the development of automated detection schemes based on three-dimensional visualization of iso-surfaces of appropriate scalar fields, such as streamwise vorticity (Jimenez & Moin 1991), vorticity magnitude (Kim 1987) and enstrophy or instantaneous Reynolds stress (Lin & Brasseur 1990). Robinson (1991*a*) has extensively used the fluctuating pressure field in this capacity, finding it to be the most reliable marker of vortical structures among the various approaches. Moin & Kim (1985) and Moin (1987) have also used three-dimensional vorticity lines to identify and study vortices.

Though Robinson found a remarkable concurrence between pressure minima and vortices, the relationship is not necessarily one-to-one (Kim 1989). Particularly in regards to weak yet growing structures close to the wall, including the region of principal Reynolds stress production considered herein, the associated pressure signatures are largely indeterminate. An illustration of this point will be given below. In addition, the pressure field is not well suited to tracking individual structures whose intensity may be rapidly changing in time. For these reasons visualization based on pressure iso-surfaces poses significant obstacles to observing the full range of vortex interactions and creation events near the boundary, and is thus not well suited for the present purposes. A more satisfactory approach is suggested by previous analyses of turbulent vortices by Spalart (1988), Lyons *et al.* (1989) and Robinson (1991*a*) among others. In this, the vortices are deduced from their imprints on two-dimensional end-

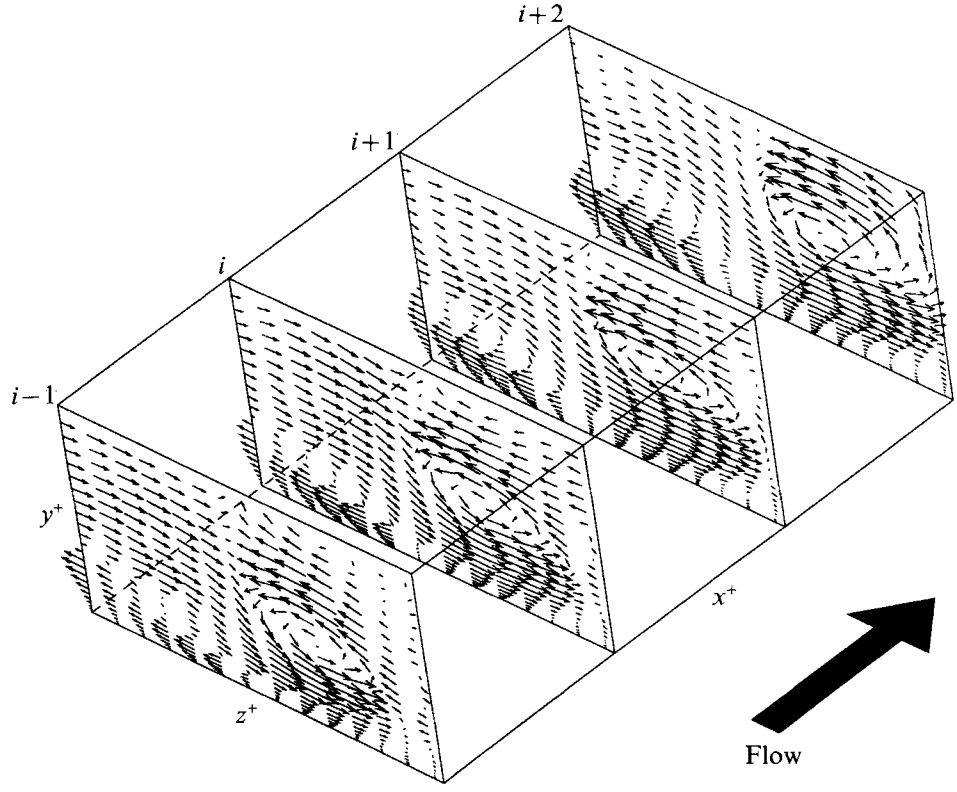

FIGURE 1. Consecutive end-on velocity vector plots.

on views of the velocity field. This approach has also recently been adopted by Brooke & Hanratty (1993) in identifying individual vortices in channel flow.

Figure 1 illustrates how the (v, w)-velocity vectors in (y, z)-grid planes can clearly and unambiguously mark the presence of vortices containing a non-negligible streamwise vorticity component. A quasi-streamwise vortex can be positioned within the flow by stringing together in the streamwise direction its local centres of rotation in the (y, z)-grid planes. Vortex selection from this point of view has the virtue of conforming to the definition of vortical structure as put forth by Robinson (1991*a*). In fact, it is this facet of vortices which is used as a final arbiter in deciding whether or not the structures found by other methods are indeed vortices.

The locations of vortex centres on given (y, z)-planes are determined here using specially developed interactive computer software. In this, an image of the (v, w)-velocity vectors at a given x-location – taken from one of the stored data sets of the complete velocity field at a particular time – is first displayed on a computer screen. Next, the cursor is directed to the vicinity of each vortex, and the algorithm illustrated in figure 2 is activated to search out the (y, z)-coordinates of the centre of rotation. The latter point is regarded as the intersection point of lines representing the loci of points where v and w change sign along the horizontal and vertical mesh lines, respectively. Once the centre of rotation of a vortex is determined, the cursor is then used to fit an ellipse, centred on the vortex axis, over the core region of the structure. An illustration of the covering ellipses found this way is also shown in figure 2. The estimate of the cross-sectional area provided by this method is useful for creating three-dimensional images of the vortices, and is not meant to be a precise analytical tool. It should be

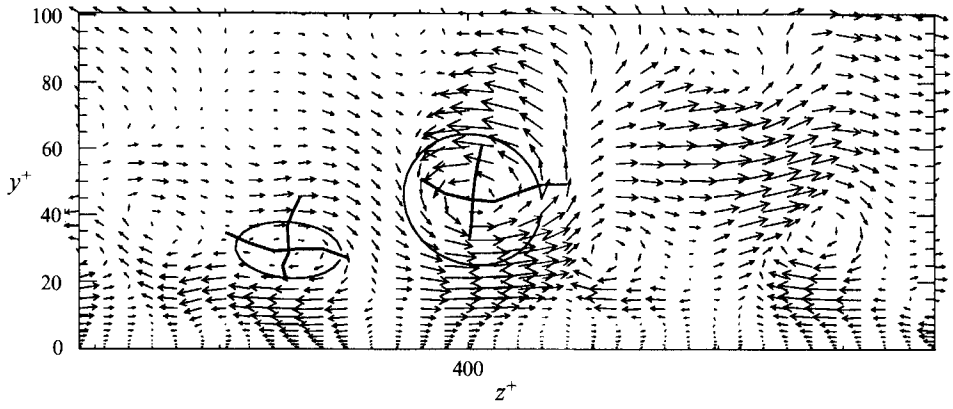

FIGURE 2. Vortex identification algorithm.

noted that the common occurrence of elliptical vortices in the end-on views is due in part to the structures lying at an angle to the streamwise direction.

Some of the vortical structures in the boundary layer are not amenable to detection through the current scheme. This is particularly true of vortices which bend either into the wall-normal or spanwise directions, as would occur for example at the top of a horseshoe vortex or arch (Robinson 1991*a*). In addition, the end-on vector plots occasionally expose the presence of complex interactions between several vortex elements, sometimes including spanwise shear layers, where the velocity vector patterns rapidly change in consecutive end-on views. Under these conditions it can be difficult to follow individual structures without ambiguity. For the purposes of the present work, vortices on consecutive planes are linked only if a relatively clear connection between them can be established so as to avoid assuming too much about the structures. As a result, it is conceivable that there are separate vortices in our analysis which should actually be parts of the same structure. While the presence of arch-like vortices and complex vortex interactions can pose a problem in so far as visualizations of the vortices is concerned, it does not appear that their presence seriously impedes our analysis of the vortex dynamics, nor our eventual conclusions about the Reynolds-stress-generating motions.

The ensuing analysis is based on a simulated channel flow at Reynolds number $R_\tau = U_\tau h/\nu = 125$ where U_τ is the friction velocity, h is the channel halfwidth and ν is the viscosity. The simulation program (Handler, Hendricks & Leighton 1989) uses the time-splitting scheme incorporating Green functions developed by Marcus (1984) as implemented by Azab & McLaughlin (1987). A mesh with $32 \times 65 \times 64$ points in the streamwise, wall-normal and spanwise directions, respectively, is used on a computational domain of size $625 \times 250 \times 625$ expressed in wall units. These dimensions are kept relatively small to reduce the formidable labour needed in getting the complete set of structures as well as the ensembles of backward particle paths needed in the transport analysis.

To insure that the box size is not a factor affecting the nature of the computed vortices, the vortex detection scheme was applied to a single timestep of a simulation incorporating a $96 \times 97 \times 96$ grid on a box of size $1822 \times 290 \times 683$ with $R_\tau = 145$. As will be shown below, no obvious qualitative difference between the vortical structures extant in each of the two simulations was found. In either case, the largest structures tended to be no more than 500 wall units long, as was also observed by Robinson

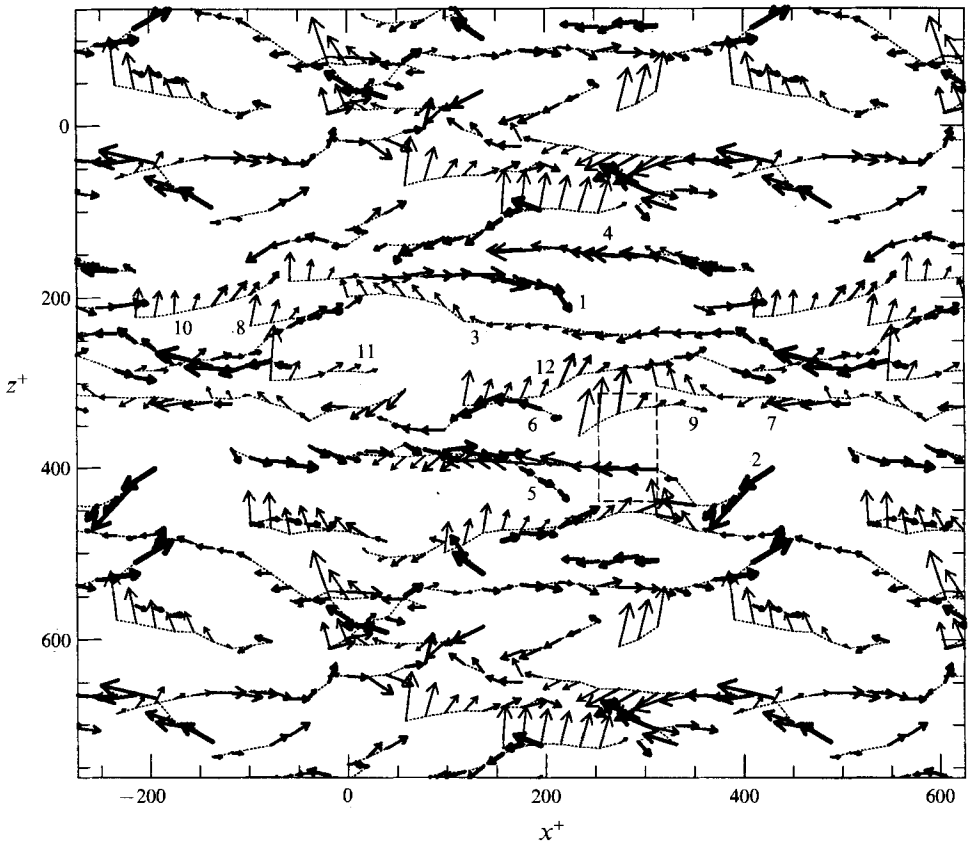

FIGURE 3. Visualization of vortical structures in plan view using axial vorticity vectors. Small dashed region corresponds to the view in figure 1.

(1991*a*) in his boundary-layer study. The great majority of quasi-streamwise vortices are much shorter than this.

3. Quasi-streamwise vortices

The complete set of vortices identified by the present scheme at a fixed time is shown in figure 3. The vortices, which are shown in plan view with a depth of field $0 \leqslant y^+ \leqslant 100$, are depicted in the form of collections of arrows constituting the (Ω_1, Ω_3) projections of the instantaneous vorticity vectors evaluated at the centres of rotation. The thickness of the arrows reflects the local height of the structures from the wall, with the thickest lines furthest from the wall, between $y^+ = 80$ and 100, and the thinnest within $y^+ = 20$. Note that periodic extensions of the domain in the two directions is given to better reveal the full set of interactions.

The vectors plotted in figure 3 are seen to line up forming a discrete number of structures whose axes have strong streamwise coherency. Some of the vortices have been assigned numbers so that they can be matched with their depictions from the side (i.e. (x, y)-perspective), given in figure 4. Note that the x^+ locations of the vortices in this figure have been set arbitrarily in order to permit easy visibility, and do not correspond to the positions in figure 3. In agreement with many previous studies, the side perspective reveals the quasi-streamwise vortices to be often tilted with respect to the streamwise direction at an angle which increases with distance from the boundary.

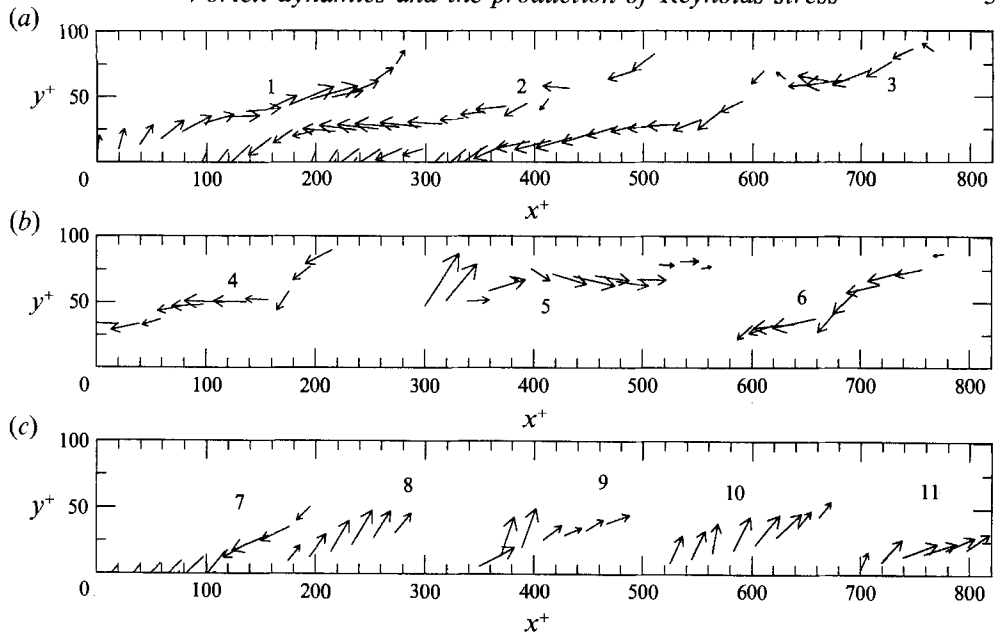

FIGURE 4. Visualization of selected vortices in side view via vorticity vectors. (*a*) Largest vortices, (*b*) outer flow vortices, and (*c*) near-wall vortices.

Most of the vortices in figure 3 lie above $y^+ = 20$ of the wall, a distance marking the outer extent of the high shear region induced by the fixed wall. At this distance the nominal spanwise vorticity is so small that the large vorticity magnitudes within the structures represent significant local perturbations above the background vorticity (Jimenez & Moin 1991). Note that the local vorticity vectors along the central axes of the vortices in figures 3 and 4, except very close to the wall, are often oriented in the same direction as the axis itself. This suggests that, at least for the region beyond $y^+ \approx 20$, the structures may be considered to be true quasi-streamwise vortices in the sense that they have fluid rotating around an elongated core region of locally high vorticity. Consequently, figure 3 implies that the present detection scheme is self-consistent, in the sense that the types of structures to which it is sensitive are ubiquitous in the region of interest. For those upstream parts of vortices situated in the high-shear region adjacent to the wall, the vorticity vectors in figure 3 have large negative Ω_3 components associated with $\bar{\Omega}_3$. These parts of the structures may be viewed more as perturbations on the background sheet of spanwise wall vorticity than discrete vortical objects.

The structures in figure 3 are shown as having definite downstream ends. These occur where, for various reasons, the vortices cannot be tracked any further from one x^+-plane to the next. Frequently, there is a fading in intensity of the vortices immediately upstream of their endpoints. This is often evident in a drop in Ω_1 as may be seen for a number of the vortices in figures 3 and 4, including those numbered 1, 3, 5, 6, 7 and 10, among others. The decrease in Ω_1 generally accompanies a tendency for the vortices to rise away from the boundary in the downstream direction while broadening in cross-sectional area. A considerable number of vortices end fairly abruptly where they are subsumed by their interaction with other vortical structures. In some cases vortices end because they rise beyond $y^+ = 100$, the limit to which vortices are tracked in this work. These must have unknown extensions in the outer flow. For an additional minority of vortices, generally beyond $y^+ = 50$, examination of the relevant (v, w)-vector plots at and just beyond their ends suggests that they are turning out of the streamwise and into

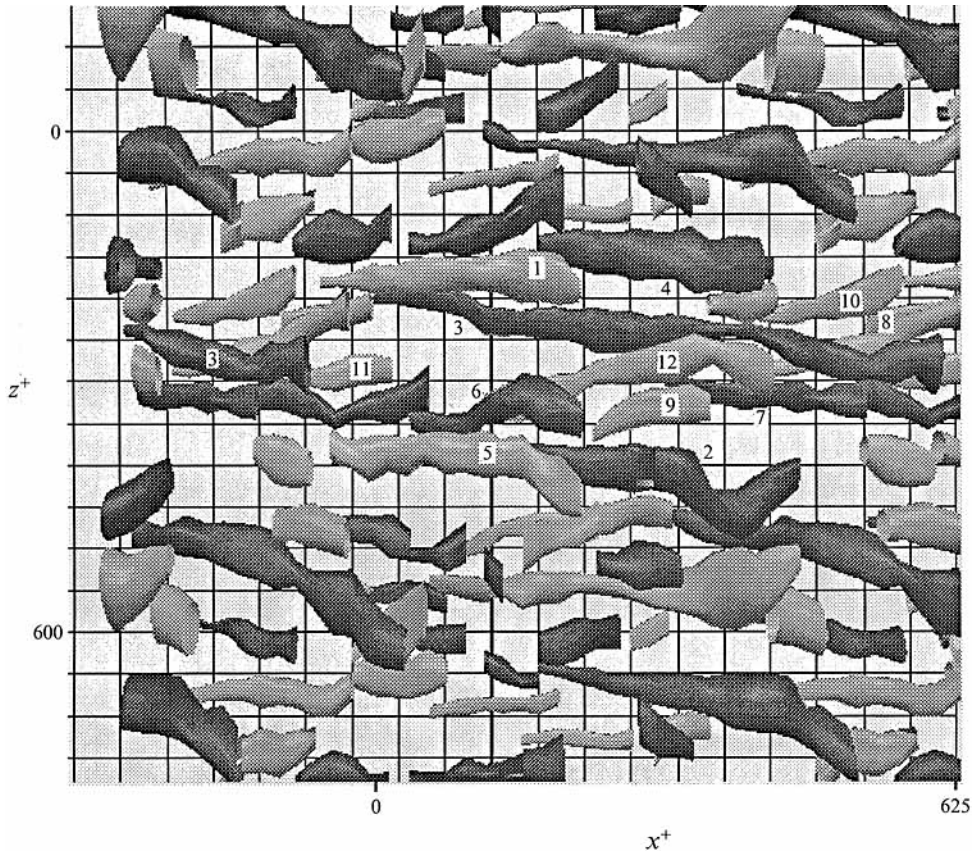

FIGURE 5. Plan view of complete set of vortices visualized using approximate core dimensions. Dark structures have negative streamwise vorticity, light structures have positive streamwise vorticity.

the wall-normal or spanwise directions. It may be concluded that the complete set of coherent vortices in the channel flow is likely to include an additional arrangement of outer flow vortices – many of which are not necessarily streamwise – besides those shown in figure 3. Furthermore, there might very well be connections between vortices which are not indicated here because their top parts are beyond the region of study or are invisible to the detection scheme. On the whole, however, the conclusion may be drawn that in agreement with Robinson (1991*a*) and Brooke & Hanratty (1993), the near-wall region, which is the main focus of our study, is almost exclusively composed of quasi-streamwise vortices, and the present detection scheme is adequate for locating the complete set of such structures.

Figure 4 is designed to make the point that the vortices can be grouped into three basic categories. Those in figure 4(*a*) are examples of the longest structures in the wall region. Their upstream ends are close to the wall and their downstream ends are in the outer flow domain. They average approximately 400 units in the x^+-direction and are very well defined, particularly in their midsections. These vortices are relatively easy to identify over many x^+-planes. In contrast, the vortices in figure 4(*b*) lie exclusively in the outer flow domain and lack extensions close to the wall. Such vortices, as well as the top parts of those in the first category, are often noticeably kinked out of the streamwise direction with jumps in magnitude and orientation of the axial vorticity vectors. The third category of structures, illustrated in figure 4(*c*), are relatively short

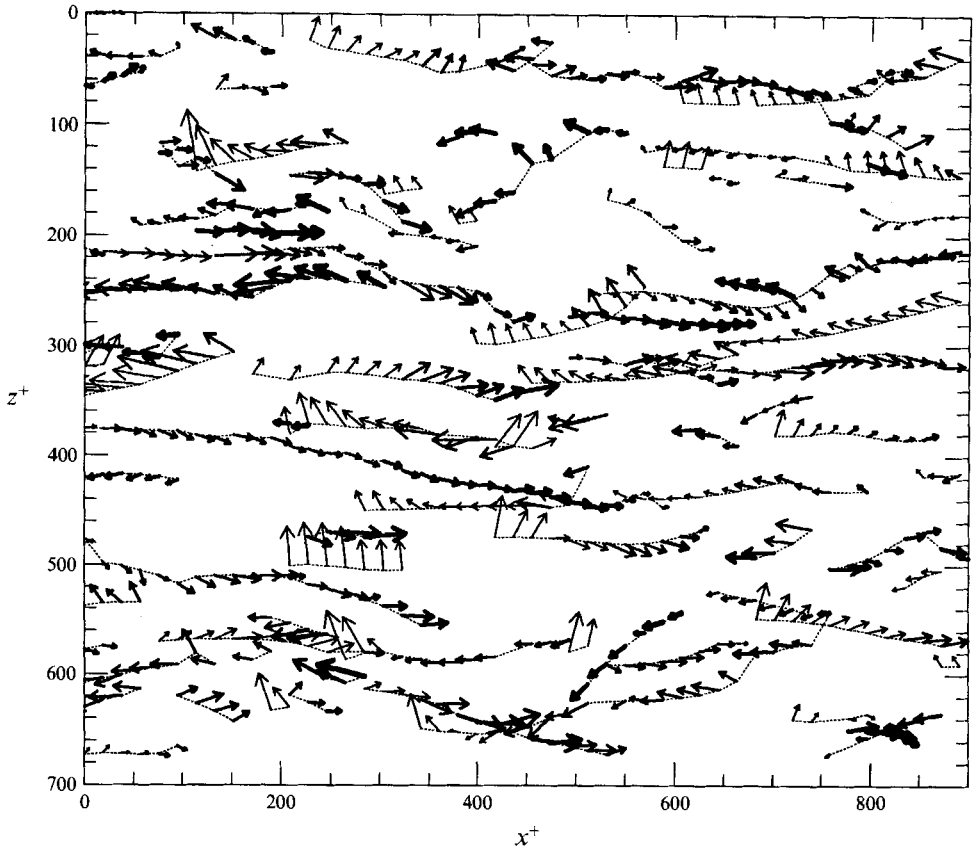

FIGURE 6. Visualization of vortical structures in $R_\tau = 145$ simulation using axial vorticity vectors.

vortices, generally less than 200 wall units in length which exist only very near the wall. These, in common with the near-wall part of the largest structures, tend to be highly coherent, relatively straight segments. Our observations of the vortex evolution process given below suggest that the group of vortices in figure 4(*c*) are relatively new, i.e. recently formed at the wall, while those in figure 4(*b*) are the remnants of mature vortices which have migrated to the outer flow. This accounts for the similar attributes of structures at equivalent distances from the wall.

A drawback of the visualization technique in figure 3 is that it downplays the extent to which neighbouring vortices may be interacting with each other. For example, vortices 2 and 9 contained in the small rectangular area in figure 3, are in fact the same ones visualized as a counter-rotating pair in the end-on velocity vector plots in figure 1. To better communicate the close interactions that vortices have with each other, it is helpful to use the information concerning vortex core size mentioned previously. The entire field of vortices displayed this way in plan view is shown in figure 5. The light shaded vortices have positive streamwise vorticity while those with dark shade have negative streamwise vorticity. The grid underlying the vortices has a spacing of $\Delta x^+ = \Delta z^+ = 50$.

Figure 5 reveals an important property of the quasi-streamwise vortices which is germane to our subsequent interpretation of the evolution process. Specifically, it shows that the upstream parts of vortices very close to the wall are often situated underneath or to the side of quasi-streamwise vortices at a higher altitude. Moreover,

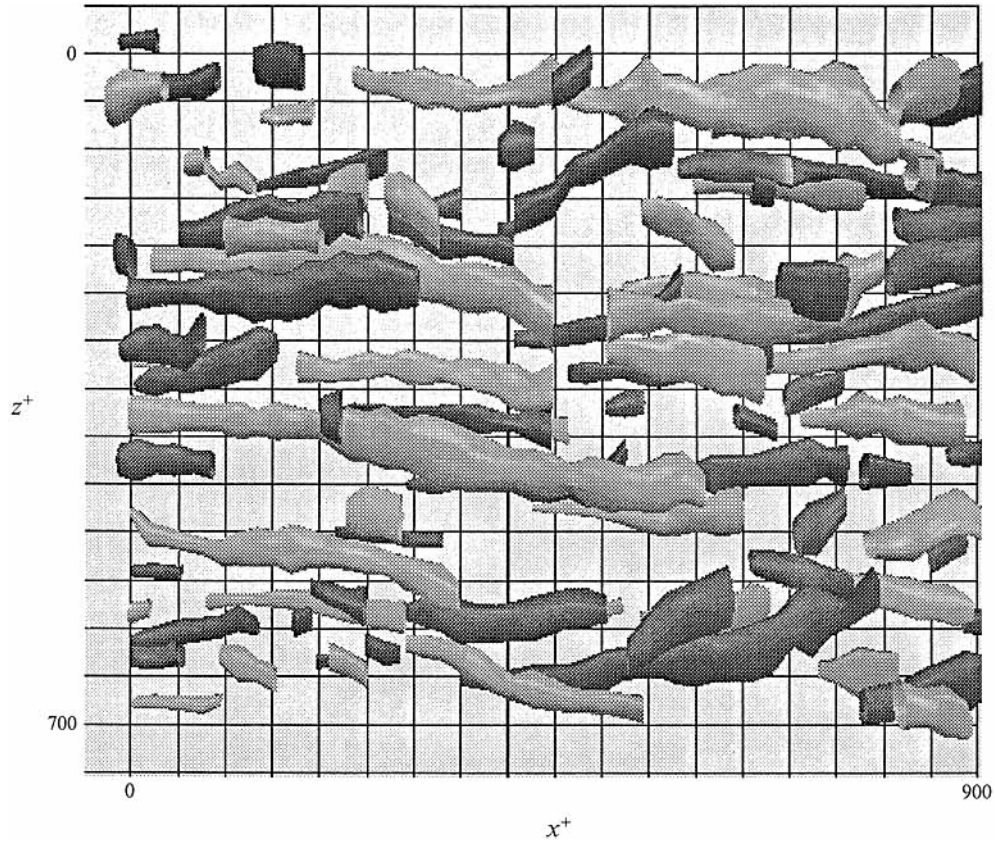

FIGURE 7. Plan view of vortices visualized using approximate core dimensions in $R_\tau = 145$ simulation.

viewed from end-on velocity vector plots, the vortices from such vertically oriented pairs are counter-rotating. Examples of this in figure 5 include the pairs (2, 5), (12, 6), (11, 3), (8, 3), (7, 9) and (3, 1) where the lower structure is listed first. Numerous other examples of this situation are contained in the figure. Below it will be shown, in agreement with Stretch, Kim & Britter (1990) and Brooke & Hanratty (1993) that at least in some cases this arrangement is a natural outcome of the generation process in which the upper vortex is primarily responsible for the generation of the lower vortex.

Figures 6 and 7 contain plots of the instantaneous field of vortices identified from the larger $R_\tau = 145$ simulation. These should be compared qualitatively with figures 3 and 5, respectively. To aid in the comparison, the domain plotted here is close to the size of that in figures 3 and 5, even though this represents only approximately half of the full plane of the larger simulation. In terms of the kinematic properties of vortex size, density, intensities, interrelationships, positions and so forth, the two simulations appear to be quite similar. Since the arrangement of vortices in these figures is most probably a strong reflection of the underlying dynamics, it is reasonable to believe that the conclusions of the present study would be unaltered if a larger simulation box size had been adopted.

It is of some interest to consider also how the structures found by the current detection scheme compare to those determined from the pressure contour method. Figure 8 shows a view of the iso-surfaces of fluctuating pressure corresponding to the same region as appears in figure 5 for the $R_\tau = 125$ simulation. The fluctuating pressure

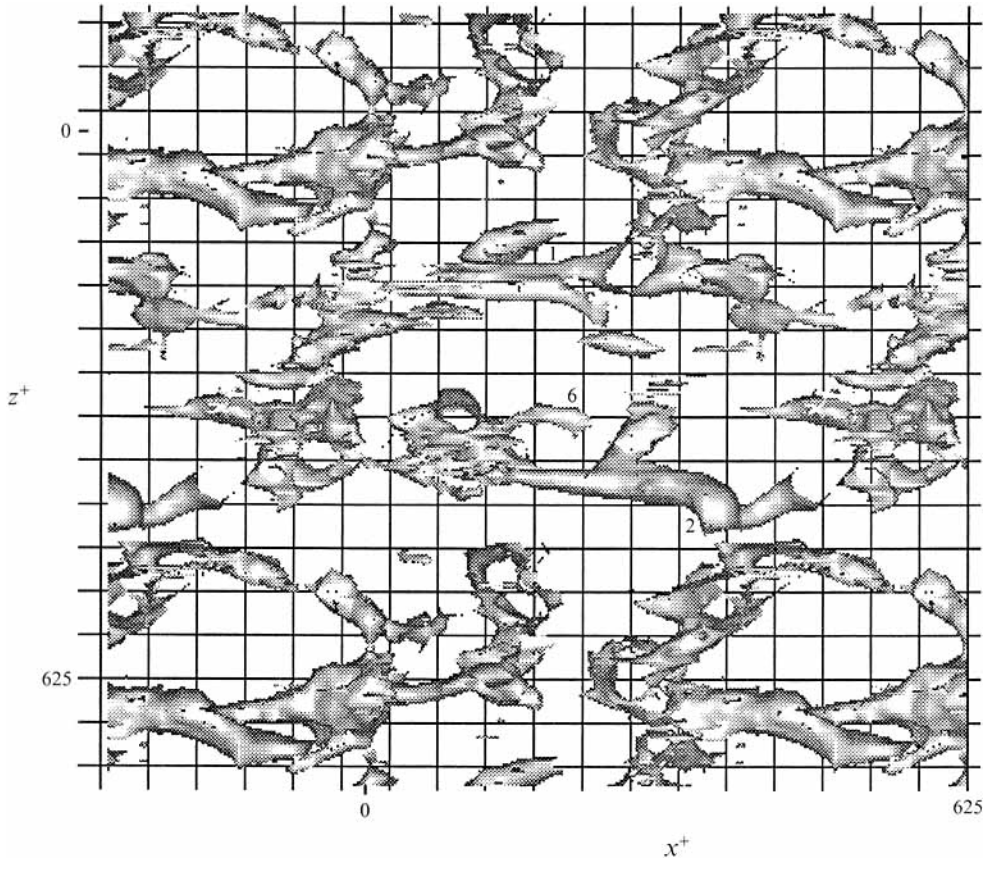

FIGURE 8. Iso-surfaces of low pressure.

contour level is $-\rho u_\tau^2$, which is chosen to provide an optimal balance between completeness and clarity. In other words, a more negative contour level eliminates structures, while a less negative value reduces their distinctness. Several of the numbered vortices in figure 5 are also visible in figure 8. Outside of these and a few additional vortices, however, the remaining structures appear to be either missed entirely or represented only in partial or distorted form. It is evident that it would be exceedingly difficult, if not impossible, to form a complete understanding of vortex dynamics solely from pressure contours. This approach may, however, be an effective means of tracking vortices in the outer flow, where the present technique is relatively difficult to apply.

4. Vortex evolution

It is likely that all stages in the development of coherent vortices in the turbulent wall region are represented in the fixed time slice of the flow in figure 5. Putting the structures into motion in time provides a means for reconstructing the sequence of events by which the quasi-streamwise vortices are maintained in the flow. The subsequent evolution of the flow field from the state in figure 5 has been computed over the interval $t^+ = 32$, in which the vortices are located and visualized at increments of $\Delta t^+ = 3.2$. This yields sufficient insight into the life cycle of the structures to be able to explore the physics of Reynolds stress production.

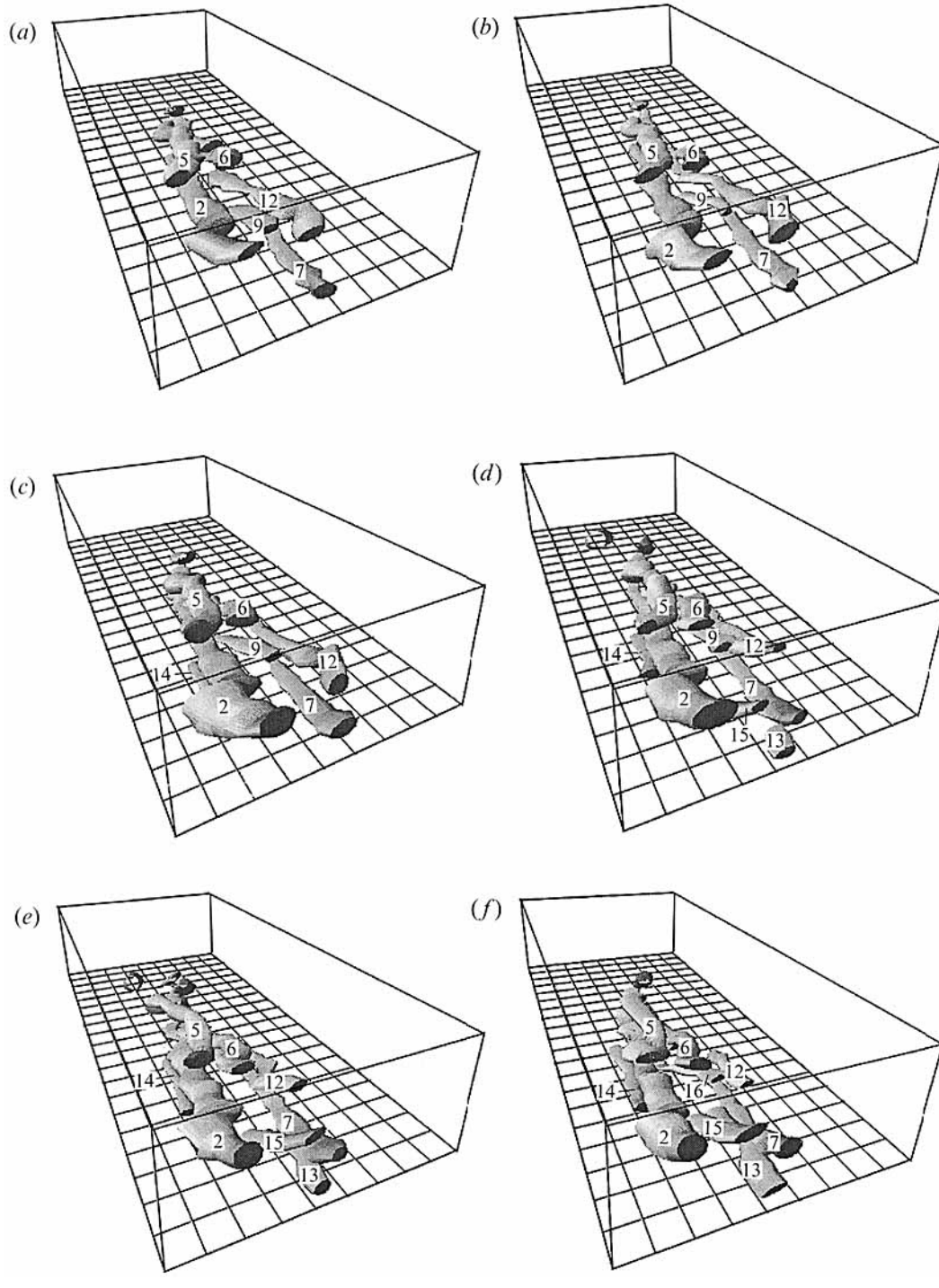

FIGURE 9. Three-dimensional visualization of vortical structures showing vortex generation. (*a*) $t^+ = 0$, (*b*) $t^+ = 6.4$, (*c*) $t^+ = 12.8$, (*d*) $t^+ = 19.2$, (*e*) $t^+ = 25.6$ and (*f*) $t^+ = 32$.

Quasi-streamwise vortices are found to originate close to the wall in response to intense spanwise shearing by pre-existing quasi-streamwise vortices (for similar results see, e.g. Chorin 1980; Lyons *et al.* 1989; Jimenez & Moin 1991; Brooke & Hanratty 1993). The new vortices, which are counter-rotating to the parent vortex, are generated often, but only by those vortices managing to bring sufficiently strong rotation to an appropriate altitude above the wall. The new structures are initially weak and short, but grow rapidly in intensity and length.

Some examples of vortex generation are illustrated in figure 9 containing the time evolution, at intervals of $\Delta t^+ = 6.4$, of a particular subset of the vortices depicted in figure 5. The viewpoint is always looking upstream from a point just ahead of the convecting group of structures. Similar events to these were recorded elsewhere in the simulation. The first new vortex, numbered 14, appears at time $t^+ = 12.8$, in response to the very strong spanwise shear associated with 2. Its birth is anticipated by an exceedingly faint rotation in the end-on views. The new vortex grows steadily, as shown in figure 10 in which the vorticity vectors on the central axis of vortex 14 are given as a function of time from plan and side views. It is particularly interesting to observe the effect of stretching in turning the vorticity vectors into the streamwise direction. Vortices 2 and 14 form a counter-rotating pair with the sense of rotation corresponding to ejection of the low-speed fluid between them. Vortex 14 has positive wall-normal vorticity, as shown in figure 10(*b*), consistent with the effect that vortex 2 would have in reorienting the local spanwise vorticity.

Figure 10(*b*) shows that the downstream end of the lengthening vortex migrates away from the wall at an inclination. This occurs because its downstream end, which is created first, rises by vortex induction at the same time that new extensions of the vortex are forming at its upstream end. In fact, it may be seen in figure 9 that the uplifted part of the vortex convects in tandem with 2 while its upstream end is continuously changing its position *vis-à-vis* vortex 2. This suggests that new parts to the vortex are being created at its upstream end next to the wall by the passage of the faster moving core of vortex 2. Further support for this process of vortex growth is the persistence of spanwise vorticity at the upstream end of the vortex as seen in figure 10(*a*).

A second counter-rotating vortex to 2, assigned the number 15, develops near its downstream end at $t^+ = 16$ and is first visible in figure 9(*d*). This vortex appears on the down flow side of 2 and also has positive wall-normal vorticity consistent with its formation by deformation of the local spanwise vorticity. The fluid between 2 and 15 has the characteristics of a sweep event. In contrast to 14, vortex 15 forms more quickly and is tilted at a steeper angle with respect to the wall. As time progresses it grows longer and higher and also overtakes the slower convecting vortex 13 becoming counter-rotating to it while still paired with 2 on its upstream end. In figure 9(*f*), at the end of the simulation, another new vortex, labelled 16, has appeared with very similar properties to 15. It also appears to be associated with a sweep event occurring between itself and 2. By their creation during sweep events precipitated by a detached vortex, vortices 15 and 16 appear to exemplify the generation process described by Brooke & Hanratty (1993). The rapidity with which 15 and 16 form on the sweep side of 2 contrasts with the more deliberate process surrounding 14. A number of other examples of this mode of vortex generation occurred during the simulation time, suggesting that it may be more common than the ejection side event. In any case, since the arrangement of vortices in figure 5 should reflect the nature of the creation process, it is likely that the previously noted nesting of pairs of counter-rotating vortices represents the aftermath of the lower vortex having been induced by the upper.

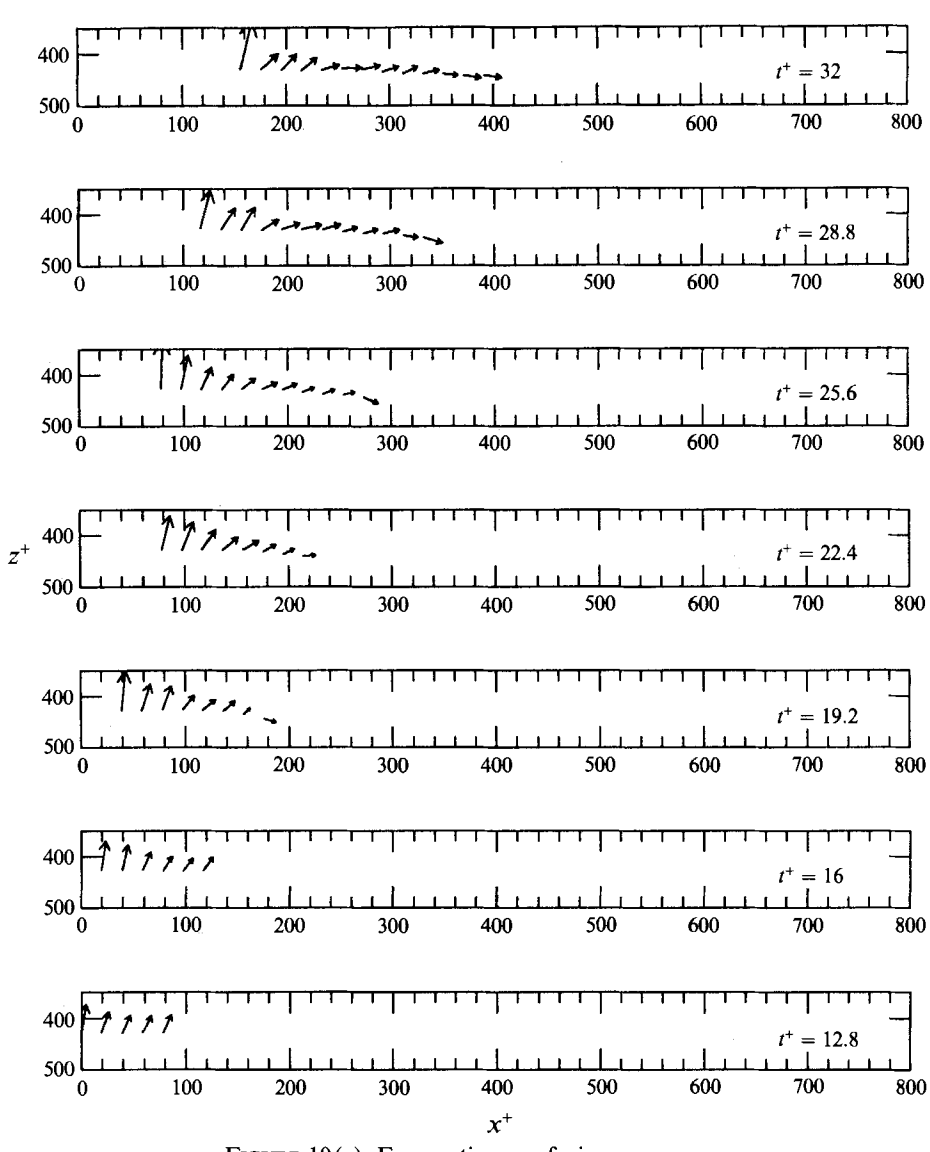

FIGURE 10(*a*). For caption see facing page.

As was mentioned previously, figures 4 and 10(*b*) show that the new vortices residing close to the wall have noticeably large wall-normal vorticity. This property may fit in with the finding of Brooke & Hanratty (1993) that streamwise shearing of wall-normal vorticity is an important means by which the strength of new streamwise vortices is enhanced. It is also evident from figures 3 and 10(*a*) that the new structures have very large spanwise vorticity as well, so that their wall-normal vorticity may, in fact, originate in the reorientation of spanwise vorticity by the parent vortex.

The examples of vortex generation seen here and in other studies suggest that there is some latitude in the necessary ingredients for vortex generation by quasi-streamwise vortices, though in each case vortices are developed next to the wall in counter-rotation to existing structures. Whether or not these generative mechanisms exhaust the possibilities remains to be seen when additional data sets are computed and analysed.

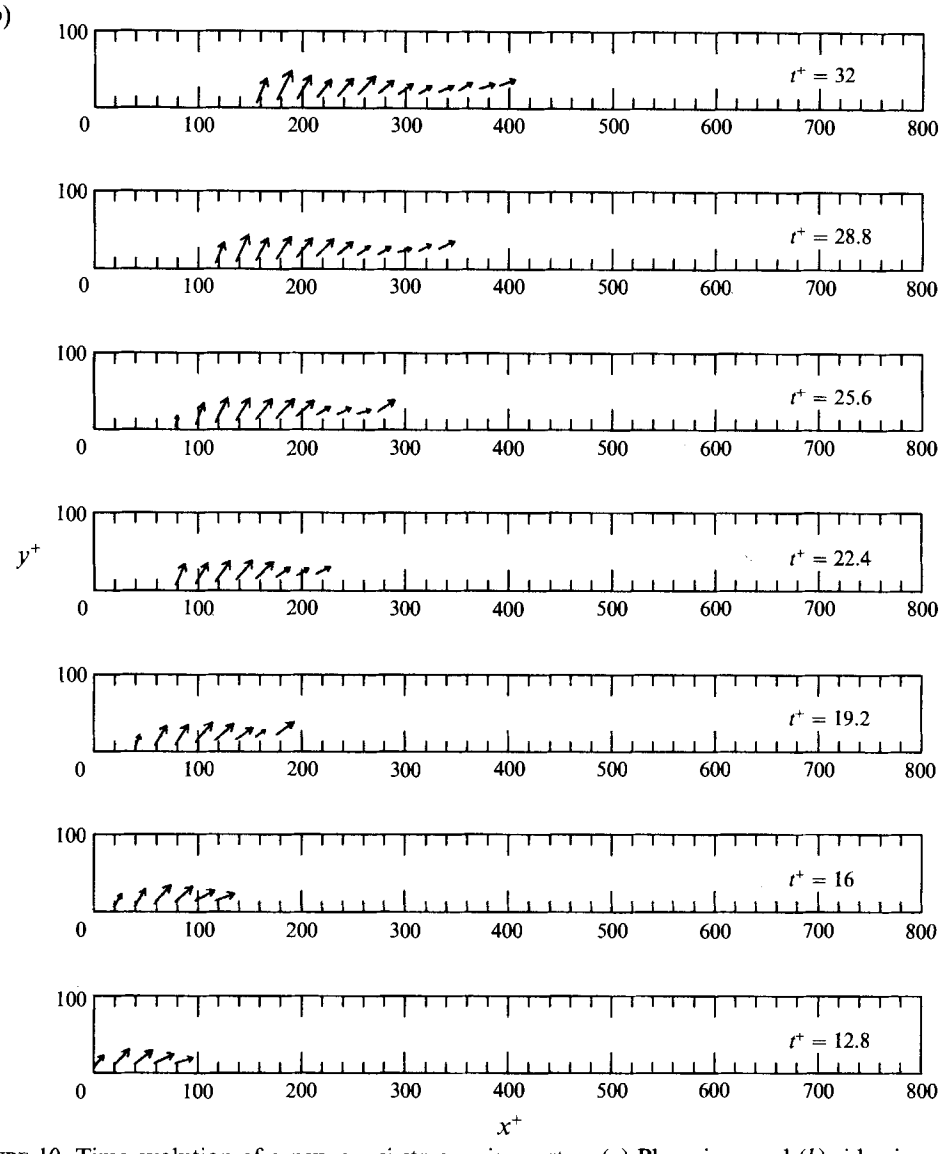

FIGURE 10. Time evolution of a new quasi-streamwise vortex. (*a*) Plan view, and (*b*) side view, of axial vorticity vectors.

Further results along these lines should also emerge once the exact set of circumstances necessary for the self-replication of streamwise vortices are understood.

Elongated and tilted vortices, such as those shown in figure 4(*a*), have very unequal convection velocities between their up and downstream ends. This must lead, ultimately, to their effective separation into near- and far-wall parts. Some evidence for this occurs in the case of vortex 2 in figure 3 and several other vortices in the simulation, though the process is not clear cut, e.g. as in a sudden division into two vortices. Rather, the upstream parts of structures appear to be left behind in a series of complex interactions with the wall vorticity, sometimes including the apparent creation of new near wall extensions of the downstream part of the vortex. It may be that this process is similar to Robinson's (1991*a*) observation that arches develop a

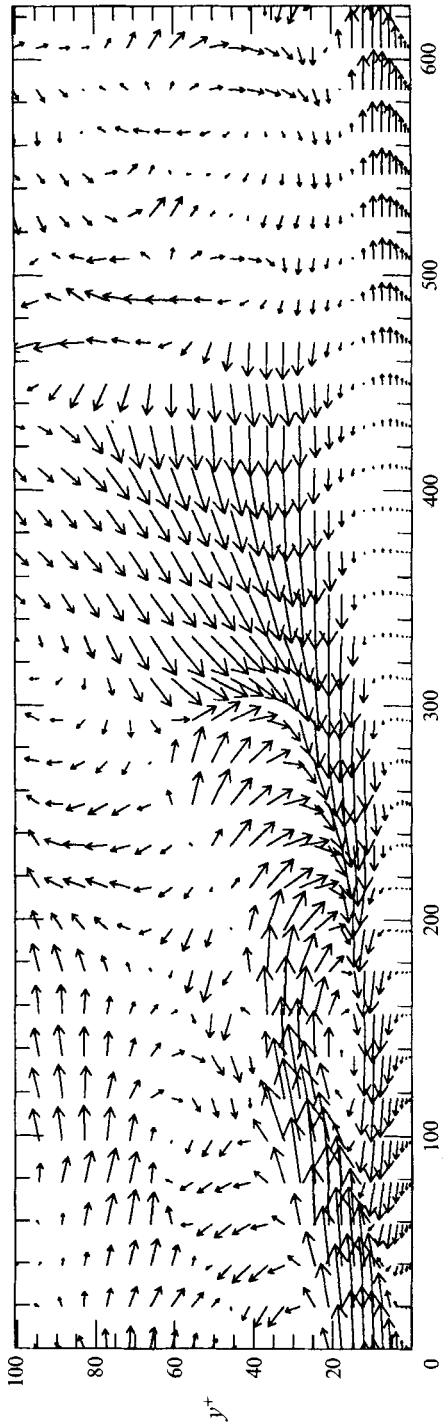

FIGURE 11. Side view of velocity fluctuation vectors at $z^+ = 393$.

series of growing and dissipating legs as they convect. It is likely that some of the highly stretched vortices manage to become completely free of the wall, as was suggested by Lyons *et al.* (1989) and Brooke & Hanratty (1993), thus accounting for the types of structures seen in figure 4(*b*).

The rapidly convecting large structures in the outer flow tend to kink into the spanwise and wall-normal directions. For example, kinking of vortex 2 so that part of it comes closer to the wall appears to be a prelude to the roll-up of vortex 14 discussed previously. The reorientation of streamwise vortices into the spanwise and wall-normal directions is achieved through inherent vortex instabilities (Chorin 1982) and Bio-Savart interactions with other structures, sometimes in the form of counter-rotating pairs. These observations, taken with the conclusions of the previous paragraph, suggest that a source of the spanwise vortices or 'arches' populating the outer flow as observed by Robinson (1991*a*) lies in the migration and shearing of quasi-streamwise vortices created at the wall.

The similarity between arch-like structures and the outer flow vortices is also suggested by the (u, v)-velocity vector plot shown in figure 11. The view is of a streamwise cut at $z^+ = 393$ through the quasi-streamwise vortex 2 in figure 3 near $x^+ = 150$. This velocity field is strongly reminiscent of similar pictures of arches given by Robinson (1991*a*) used in illustrating the transverse roll-up process. Here, however, the vortex is a quasi-streamwise vortex which is only slightly transverse to the streamwise direction.

Examination of the evolving vortices in the simulation gives the overriding impression of a continual and rapid change in the panorama of mutual interactions. This is partly a result of their convection at different velocities, so that any individual structure, or part of a structure, encounters a dynamically varying set of neighbours. As vortices of opposite streamwise rotation come near they have the capacity to form localized regions of counter-rotation which can visibly increase in intensity in a short time. Depending on the match up of vortices, either ejections or sweeps are possible. In some cases, ejections and sweeps occur from the same counter-rotating pair as the individual vortices twist around each other in helical formation. An example of this phenomenon will be seen below in a different context.

It should also be mentioned that several vortices are observed to vanish or become significantly reduced in stature during the course of the simulation. These enter the calculation as relatively weak vortices, and either fade away owing to diffusion or become unrecognizable owing to the imposition of other structures. Not surprisingly, approximately the same number of vortices are lost during the time period of the simulation as are created.

5. Relationship to wall pressure

The pressure field on bounding surfaces in turbulent flow has been the object of considerable interest owing to its importance in fluid/structure interactions, sound generation, cavitation and so forth. A prominent feature of the wall pressure field, which has been observed in physical and numerical experiments, is the presence of rapidly translating local pressure maxima. It is widely suspected that these reflect the passage of vortices overhead, though it has not been clear whether near- or far-wall structures are the cause. Kim (1989) has concluded from an analysis of space/time correlations that the pressure maxima are formed from vortices travelling near the wall. Strong evidence for a kinematic relationship was recently obtained by Robinson (1991*a*) in which iso-pressure surfaces were used to mark the structures. In view of

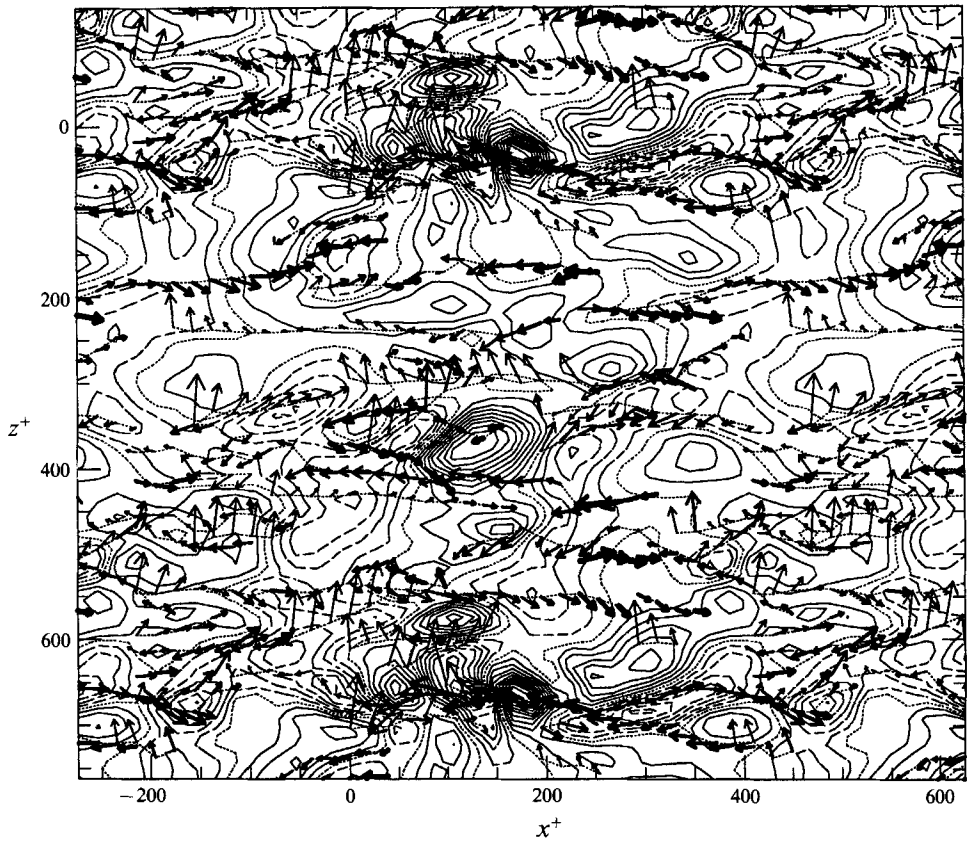

FIGURE 12. Contours of wall pressure superimposed on the complete set of axial vorticity vectors at $t^+ = 32$.

these results, it is of some interest to examine the relationship between the vortical structures selected here and the surface pressure field.

Figure 12 shows the complete set of vortical structures at $t^+ = 32$ superimposed on the wall pressure contours. The strong correlation between these two fields is particularly evident in the tendency of the locations of maximum pressure to adhere closely to the sweep sides of the vortices. More dramatic evidence linking the pressure and vortices is given in figure 13 showing the time evolution of the pressure field prior to the appearance of the major pressure peak in figure 12 at $x^+ = 150, z^+ = 350$. The view is of a streamwise slice of the plane containing the pressure contours together with a single convecting vortical structure, namely, vortex 2 in figure 3. For figure 13, time increases in intervals of $\Delta t^+ = 6.4$ from $t^+ = 0$ in the top view to $t^+ = 32$ in the bottom view. Examination of the associated end-on velocity vector plots confirms that the vortex shown in the figure is the only one affecting the location where the peak pressure lies.

Figure 13 suggests that the pressure peak in question evolves owing to an inrush of fluid to the wall caused by the convecting vortical structure. In particular, tracing backwards from the final picture in figure 13 (which contains the peak shown in figure 12), it is clear that the rise in intensity of the pressure disturbance coincides with the passage of the vortex. The sweep of fluid towards the wall associated with the pressure peak commences near the downstream end of the structure as seen in the top figure. A second pressure maximum, appearing to have a very similar history and explanation

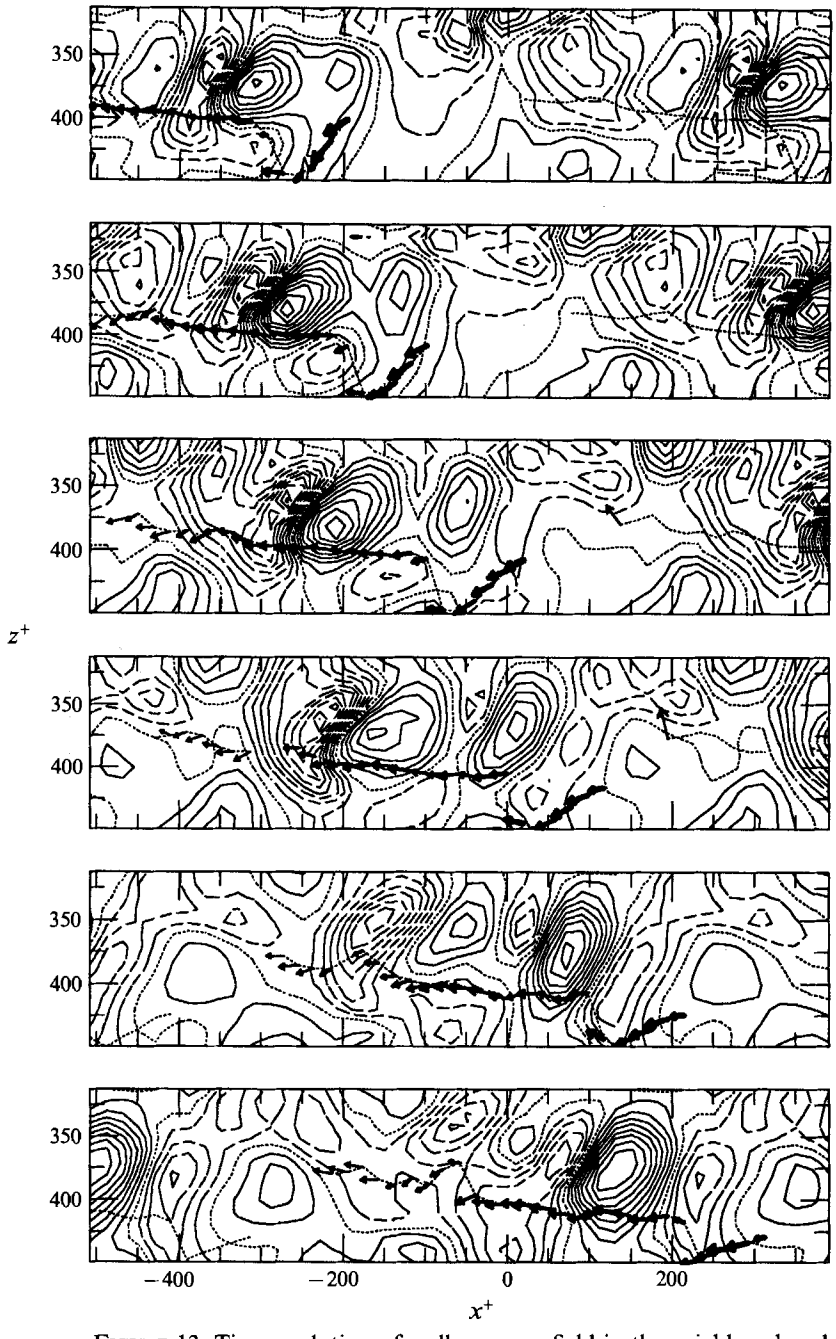

FIGURE 13. Time evolution of wall pressure field in the neighbourhood of a convecting vortical structure.

to the first, is also visible in the figure. The maximum pressure in this case is reached at $t^+ = 6.4$ followed by its subsequent rapid dissipation. The very beginning of the creation of a third pressure peak is also evident in the last few scenes of figure 13, in the region just ahead of the structure.

A substantially equivalent dependence on the underlying vortical motion was found to pertain to each of the other pressure peaks in figure 12. The conclusion may be

drawn that the wall pressure field is largely a phenomenon associated with near-wall vortical structures, developing in direct and immediate response to the fluid motions they generate. That the collection of quasi-streamwise vortices found here can account for such dynamically important aspects of the flow as the wall pressure maxima, is additional evidence suggesting that no important structural features of the wall region flow field have been overlooked by the present detection scheme.

6. Reynolds stress generation

We now consider the mechanisms by which the Reynolds stress is produced from the evolving vortex system described in the previous sections. Our intent is to develop a dynamical explanation for the well-established kinematical connection between vortices and regions of intense instantaneous ejection and sweep activity. Our principal means of linking vortex evolution with the physical processes affecting Reynolds stress is through the intermediary of ensembles of fluid particle paths carrying dynamical information about the physics of Reynolds stress production.

The paths utilized in our transport analysis (see BH) are collections of backward fluid particle trajectories, i.e. paths arriving on predetermined y^+ levels after travelling for a specified time interval. From ensemble averaging over the collection of paths, the Lagrangian Reynolds stress decomposition,

$$\overline{u_a v_a} = \overline{u_b v_a} + \overline{v_a(\bar{U}_b - \bar{U}_a)} + \overline{v_a(U_a - U_b)}, \tag{1}$$

may be evaluated. Here, a refers to fluid particles randomly scattered over a fixed y^+ plane at time $t^+ = \tau$, and b is their locations at the earlier time $t^+ = 0$. The first term on the right-hand side is zero for τ large enough, thus expressing the mixing condition. When this is fulfilled, (1) reduces to

$$\overline{u_a v_a} = \overline{v_a(\bar{U}_b - \bar{U}_a)} + \overline{v_a(U_a - U_b)}, \tag{2}$$

where the decomposition of $\overline{uv}$ is now into displacement and acceleration transport given by the first and second terms on the right-hand side, respectively. Evaluation of (1) was made in BH using ensembles of particles computed from the channel flow simulation described previously at $R_\tau = 125$. In this, the interval $\tau^+ = 32$ proved to be sufficiently long for u_b and v_a to be decorrelated. The computed values of the displacement and acceleration transport terms show that the former dominates the Reynolds stress in the near wall region, though acceleration effects are not negligible. In fact, they account for approximately 20% of Reynolds stress in the region $20 \leqslant y^+ \leqslant 40$.

For the present study we consider two groups of 1000 paths each arriving after $t^+ = 32$ at the levels $y^+ = 7.3$ and 24.6 on one particular side of the channel. The plane $y^+ = 7.3$ is one where sweep events predominate and $y^+ = 24.6$ is one where ejections are most prevalent, so that by studying conditions at these two levels we can attain a relatively complete view of the different facets of Reynolds stress generation. The basic premise of the ensuing analysis is that the entire dynamical content of the Reynolds stress, at each of the y^+ positions studied, is contained within the appropriate ensemble of 1000 particles. Since at each y^+ level individual particle paths in the ensemble can be ranked according to the magnitude of their contribution to displacement and acceleration transport, we thus have the means by which to determine the most significant Reynolds stress producing events in the flow.

Examination of the individual contributions to $v_a(\bar{U}_b - \bar{U}_a)$ at $y^+ = 7.3$, shows that the top 134 of 1000 paths contribute an amount equal to the total displacement transport at this location. The remaining particles have contributions which can be

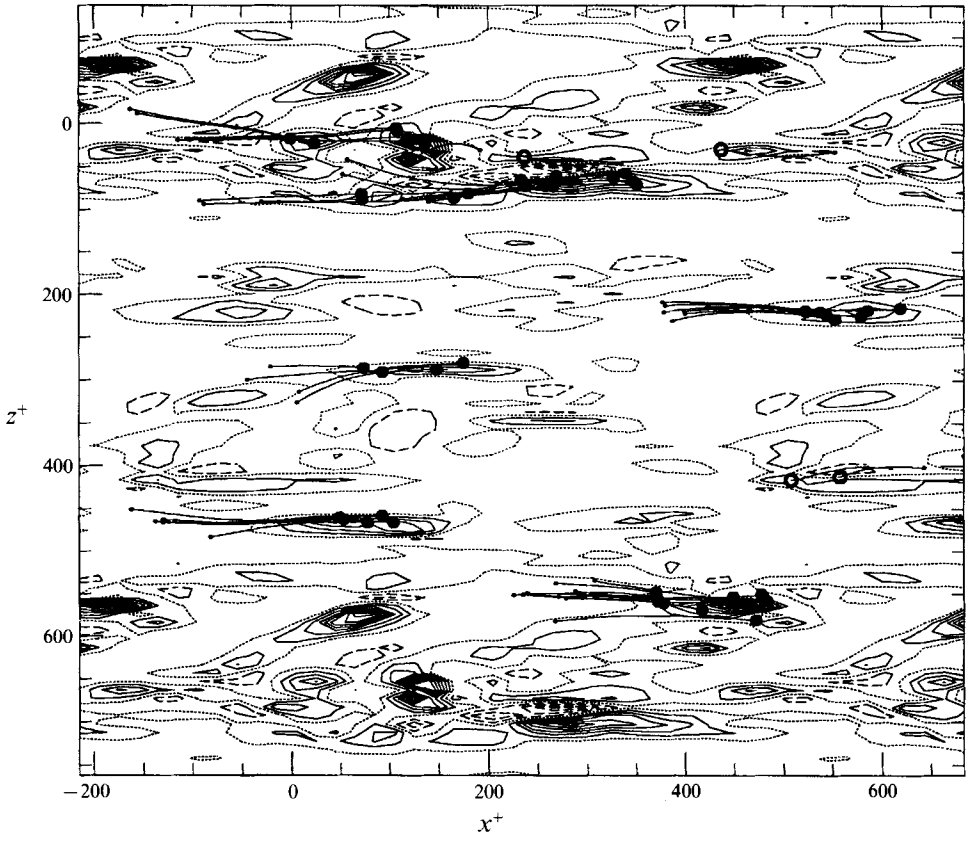

FIGURE 14. Plan view of the 50 paths contributing the most to displacement transport at $y^+ = 7.3$, superimposed on contours of $\phi = uv - \overline{uv}$. ——, $\phi < 0$; ....., $\phi = 0$; ——, $\phi > 0$; ●, particles at $t^+ = 32$ with $v_a < 0$; ○, particles at $t^+ = 32$ with $v_a > 0$; •, positions of particles at $t^+ = 0$.

thought of as cancelling between positive and negative values. A very great majority of these, in fact, contribute very little to transport in an absolute sense. The situation is similar for displacement transport at $y^+ = 24.6$ and for the acceleration transport term as well. It follows that we can frame our study of the Reynolds stress dynamics in terms of the large contributions of a relatively small fraction of the total set of particles.

Figure 14 is a plot of the 50 paths contributing the most to displacement transport at $y^+ = 7.3$ superimposed on contours of the Eulerian field $\phi \equiv uv - \overline{uv}$. The trajectories of the fluid particles in figure 14 are plotted as they would be viewed by an observer travelling at the mean velocity at $y^+ = 7.3$. The ending points of the fluid particles are denoted by large circles: filled in for particles travelling down toward the wall and open circles for particles travelling away from the wall. The initial points of the particles, which are not generally on the ending plane, are denoted by the small solid circles. Fluid particles in sweeping motions appear to be travelling to the right since they are faster moving than the observer at $y^+ = 7.3$. Conversely, ejecting particles look as if they were travelling from right to left since they tend to come from closer to the wall before arriving at 7.3 and thus travel slower than the observer. The solid contours denote the locations where $\phi < 0$, i.e. uv is more negative than the Reynolds stress $\overline{uv}$. In agreement with earlier studies, ϕ is seen to achieve exceptionally negative values in widely dispersed regions of small support.

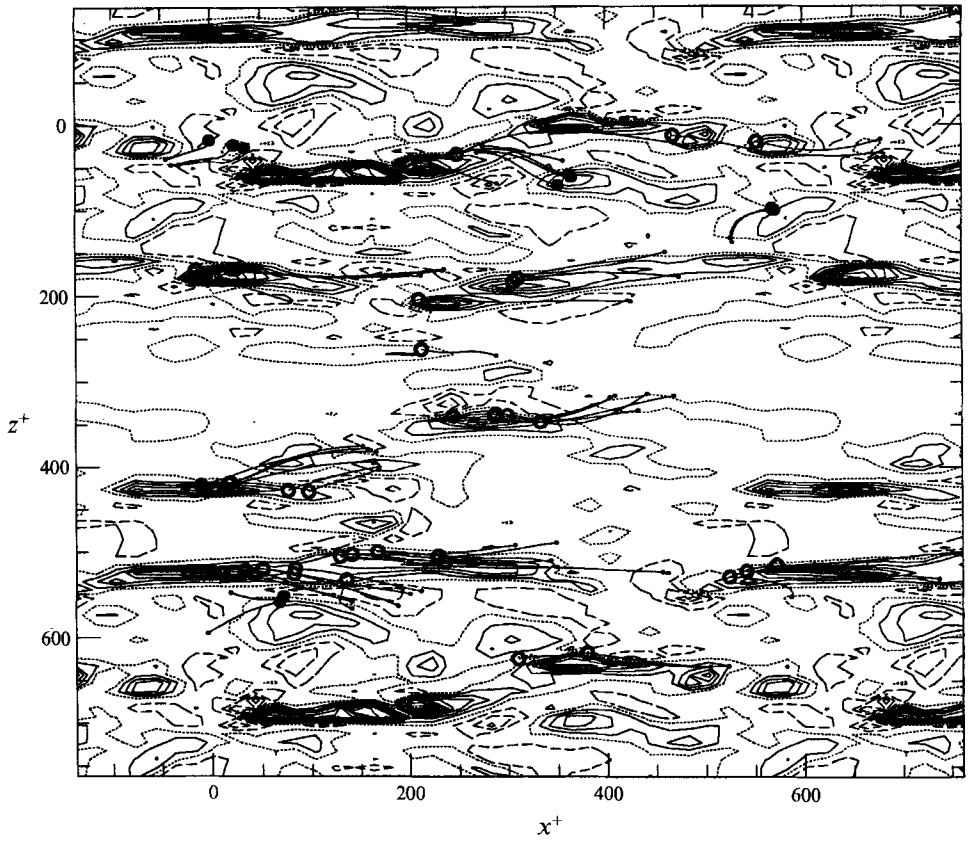

FIGURE 15. Plan view of the 50 paths contributing the most to displacement transport at $y^+ = 24.6$, superimposed on contours of ϕ. Notation is as in figure 14.

Not unexpectedly, virtually all of the 50 paths in figure 14 are sweeps. A striking aspect of the figure is the extent to which the most significant paths occur in tightly bunched groups conforming precisely to the regions of very intense instantaneous Reynolds stress. This may be taken as further justification for assuming that the crux of Reynolds stress generation depends on a relatively small number of spatially isolated events, whose dynamical characteristics are recorded in the motions of a small fraction of the full ensemble of particles. In the case of figure 14 it should be remarked that a plot of the entire set of 134 particles, contributing 100% to displacement transport, is not substantially different from the view depicted here, i.e. the paths are still mostly congregated in the same few isolated locations.

An equivalent plot to figure 14, but for the paths ending at $y^+ = 24.6$, is shown in figure 15. Here the predominant contribution to displacement transport is through ejections, though a few sweeps are also visible. As before, Reynolds stress generation is concentrated in a few localized centres, though these tend to be somewhat more extended in the streamwise direction than at $y^+ = 7.3$.

To complete this survey of Reynolds-stress-producing activity, the 50 top contributions to acceleration transport at $y^+ = 24.6$ are given in figure 16. We need not show the similar case at $y^+ = 7.3$, since there the net acceleration transport term is positive owing to the dominant effect of viscous forces in decelerating incoming sweeping motions. According to BH, acceleration transport is close to its peak

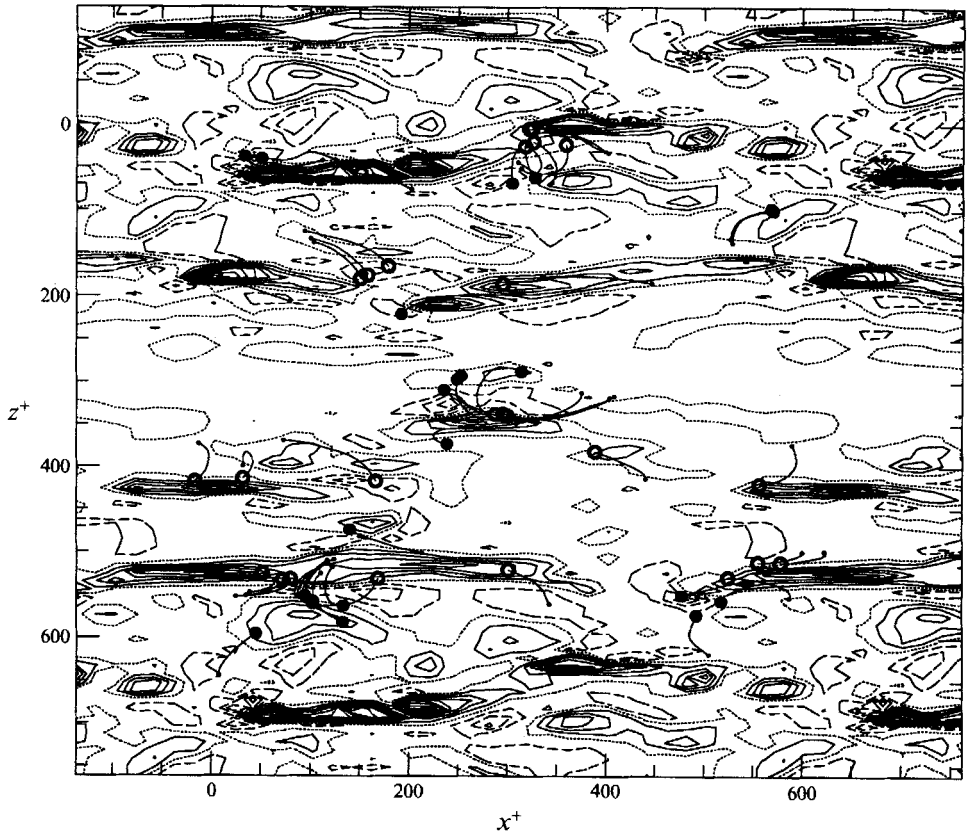

FIGURE 16. Plan view of the 50 paths contributing the most to acceleration transport at $y^+ = 24.6$, superimposed on contours of ϕ. Notation is as in figure 14.

magnitude at $y^+ = 24.6$ and the particles in figure 16 give much evidence for the presence of strong accelerations. For example, many of the particles travelling towards the wall at $t^+ = 32$ often start out slower than the observer, but finish travelling faster than the observer. Particles which are rising at $t^+ = 32$ tend to display the opposite behaviour. As in the case of displacement transport in figures 14 and 15, most acceleration events generally occur in the immediate vicinity of regions where uv is quite negative.

In view of the obvious complexities inherent in visualizing the simultaneous transient development of the entire set of vortices with superimposed particle paths, we will instead investigate this relationship through focusing on individual events in the flow which are representative of many others. This last point is to be emphasized: our ensuing descriptions of specific flow events are meant to be understood as having an echo in many more similar events transpiring in the flow field.

We first examine the intense Reynolds stress events displayed in figure 14. Among the most prominent is the sweep ending in the vicinity of $x^+ = 450, z^+ = 550$. Figures 17 and 18 show in plan and end-on views the flow environment surrounding one of the fluid particles involved in this sweep, in fact, the trajectory carrying the maximum value of $v_a(\bar{U}_b - \bar{U}_a)$ amongst 1000 particles. This value is approximately 40 times the local mean displacement transport, showing the singular importance of this dynamical event. In comparison, the least significant of the 50 top contributing particles in figure 14 is at the level of 7 times the average.

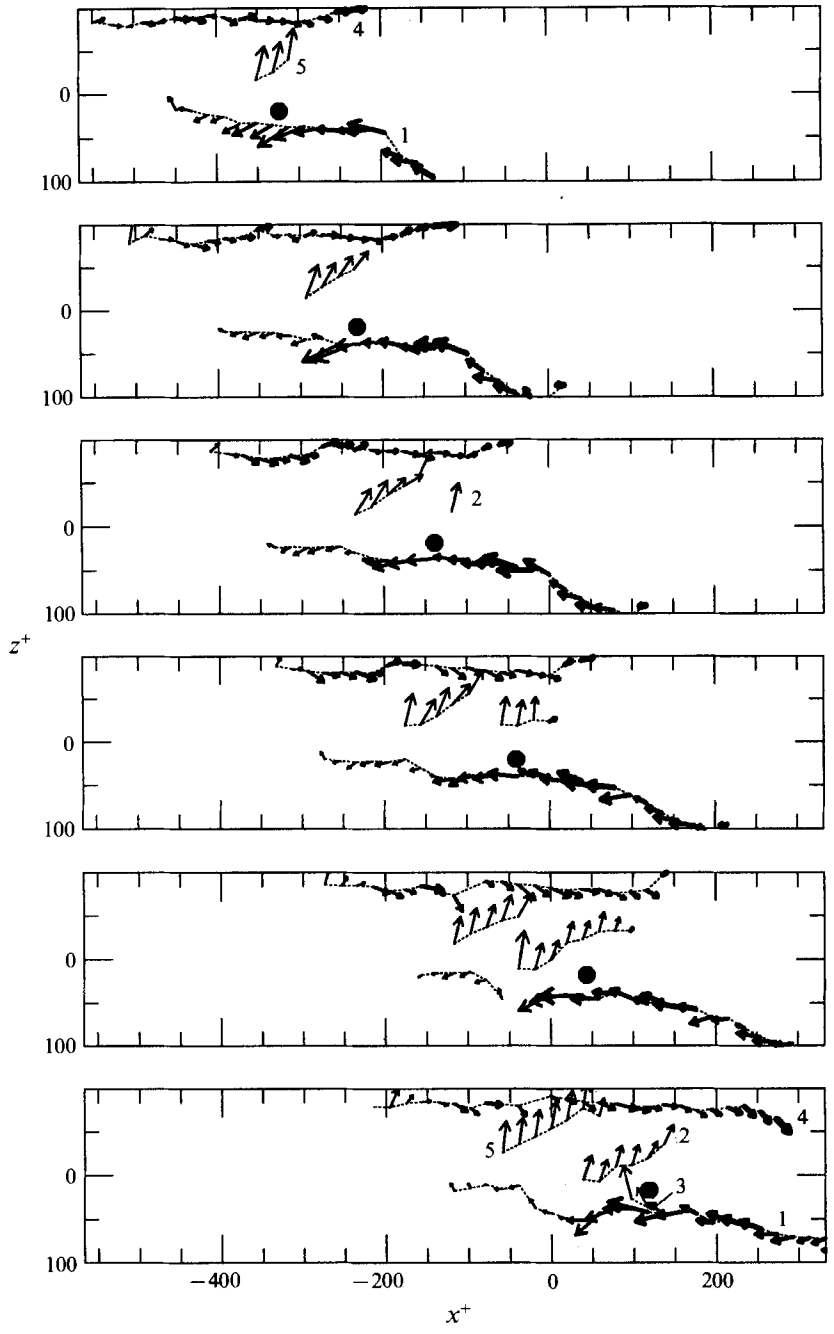

FIGURE 17. Time evolution of sweep event in plan view ending at $y^+ = 7.3$. Time increases in increments of $\Delta t^+ = 6.4$ from $t^+ = 0$ in the top figure until $t^+ = 32$ in the bottom figure.

The sequence of views in figures 17 and 18 begins in the top pictures at $t = 0$ and ends in the lower figure at $t^+ = 32$. The intermediate views are at intervals of $\Delta t^+ = 6.4$. The particle position at any time is indicated by the large circle. The vortices shown in figure 17 are limited to those having relevance to the sweep in question. These may be readily matched to the vortical motions evident in the end-on velocity vector plots in figure 18.

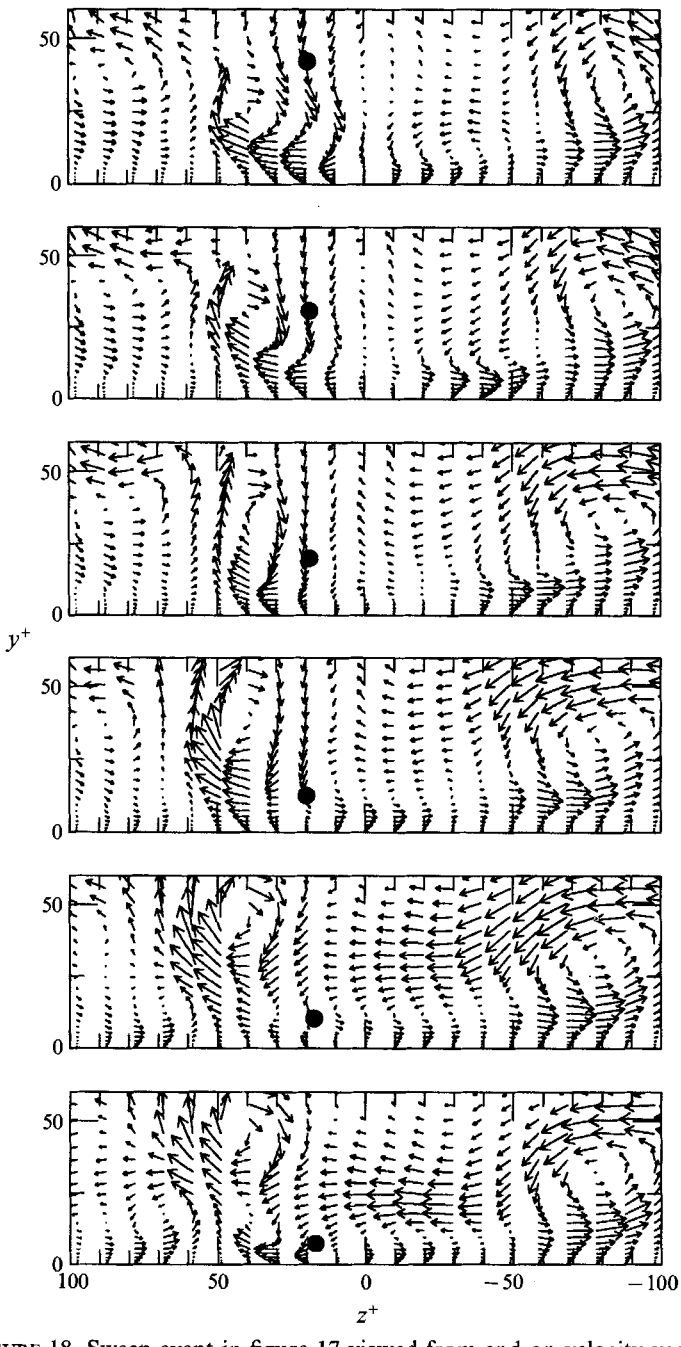

FIGURE 18. Sweep event in figure 17 viewed from end-on velocity vector plot.

The latter contain the interpolated velocity field at the x^+ position occupied by the fluid particle at each of the indicated times. Figures 17 and 18 leave little doubt that the sweep event illustrated here is the direct result of motion induced by vortex 1. During its approach to the wall, the high-speed sweeping fluid travels in tandem with the vortex, as is evident from figure 17, until its subsequent entrainment in the flow associated with vortices 2 and 3 very near the wall. The fluid particle penetrates to

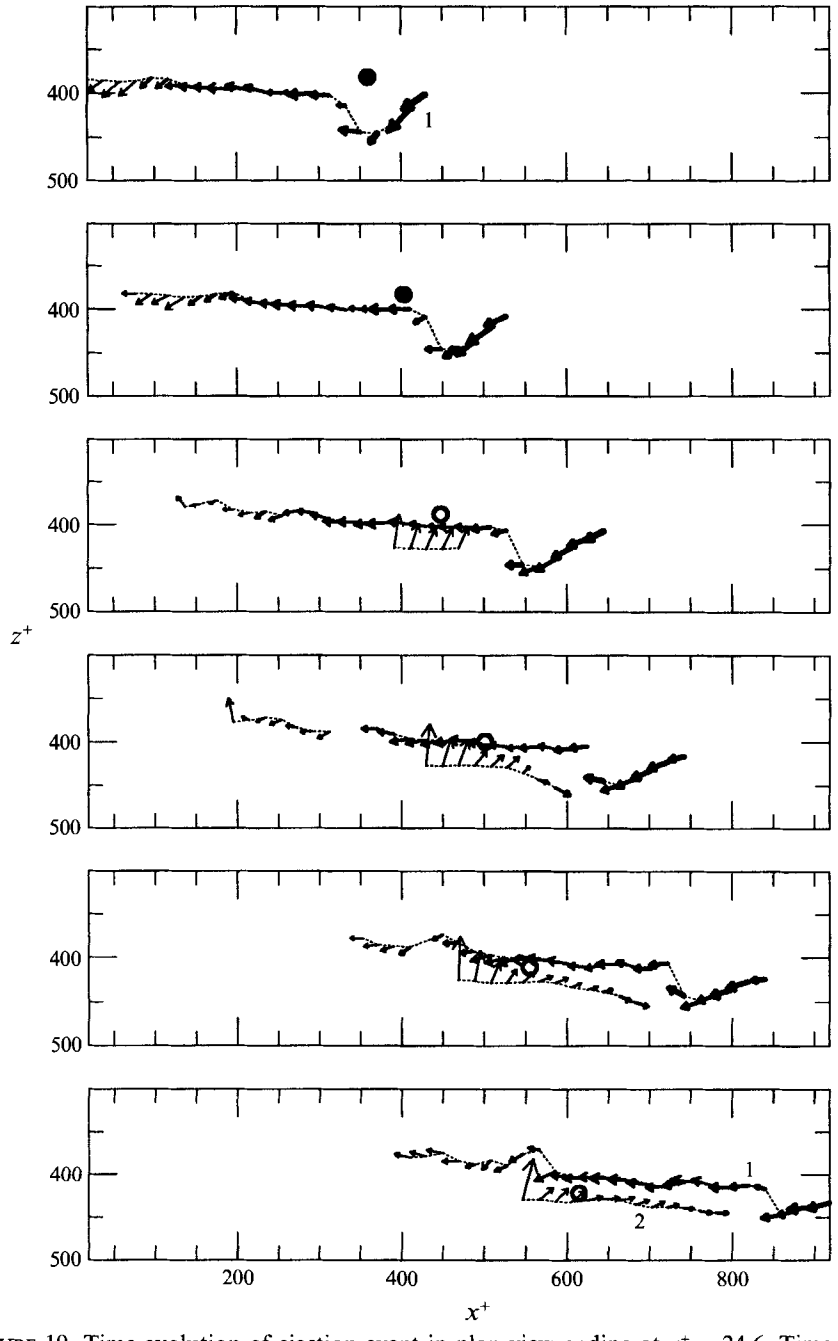

FIGURE 19. Time evolution of ejection event in plan view ending at $y^+ = 24.6$. Time increases in increments of $\Delta t^+ = 6.4$ from $t^+ = 0$ in the top figure until $t^+ = 32$ in the bottom figure.

points close to the boundary while still maintaining a relatively high streamwise velocity, thereby accounting for the intensity of the event. The rapidity of the fluid particle motion is exemplified by its rapid progress in comparison to the convection of vortex 5.

Vortices 2 and 3 appear to play a major role in the final progress towards the wall of the fluid particle shown in figure 18. Each of these vortices is newly generated in the

course of the simulation. Vortex 2 develops at $t^+ \approx 12.8$ (third picture from the top) owing to the influence of 1, with which it is in counter-rotation. Subsequently it grows to occupy a part of the region between the large-scale counter-rotating pair formed by 1 and 4. Vortex 3 develops very rapidly in counter-rotation to 2 at a location essentially underneath the point where 1 is detached from the wall. Vortex 1 is of the same sign as 3 just as 2 is of 4. Both of the new vortices form on the respective sweep sides of the generating structures in common with the vortices 15 and 16 discussed previously with reference to figure 9.

The sweep event in figures 17 and 18 clearly illustrates the role of vortices in generating Reynolds stress. Moreover, it suggests that the penetration of high-speed fluid to points close to the wall depends on the presence of strong vortical structures in the near wall region. A second example of this phenomenon exists in the sweep at $x^+ = 100, z^+ = 450$ in figure 14 resulting from the action of vortex 14 in figure 9(c–f). Close examination of the other principal sweep events in figure 14 show them also to depend on the action of intense vortices very near the wall. In these cases the structures appear to be relatively newly created, even though they did not form during the current simulation. It may be concluded from these observations that it is likely to be more than coincidental that the chief sweep producing Reynolds stress events in the near-wall region occurs where new vortices are generated. Thus, momentum transport closest to the wall appears to be a phenomenon intimately tied to the regenerative properties of the quasi-streamwise vortices, since it is primarily at the points where new vortices form that the significant wallward motions associated with Reynolds stress production can be found very close to the wall.

Considering now the case of ejections, such as those displayed in figure 15, the essential dynamical feature may be illustrated via the event occurring at $x^+ = 550$, $z^+ = 550$. Figures 19 and 20 show the relationship between the trajectory of one of the particles in this group and the local vortical structures. The fluid particle chosen, which is the second highest contributor to displacement transport at this y^+ level, has a magnitude of $v_a(\bar{U}_b - \bar{U}_a)$ which is 21 times the average. In this event, vortex 1 overtakes the slow moving fluid particle and induces it to rapidly rise up from near the wall into the outer flow. Coincidentally, the newly generated vortex 2, which was previously labelled as 14 in figure 3, enhances the ejection of the fluid particle by its counter-rotation with vortex 1.

A second ejection example is shown in figures 21 and 22 which is meant to highlight the connection between counter-rotating vortices and Reynolds stress production. In this event, located at $x^+ = 200, z^+ = 50$ in figure 15, the contribution to Reynolds stress is the largest among those in the ensemble at this location, being 25 times the average. The time sequences in figures 21 and 22 shows the entrainment of the fluid particle near the wall into vortex 1, followed by its rapid ejection between the counter-rotating pair formed by 1 and 2. In this instance vortex 2, which is further from the wall than 1, convects much faster, overtaking the lower vortex. This sets up the interaction between the vortices in the form of appreciable counter-rotation with the consequent ejection of the fluid particle from between them and the production of Reynolds stress. The last few scenes in figures 21 and 22 serve to illustrate a point made earlier to the effect that counter-rotating vortices can induce both ejections and sweeps if they are coiled around each other.

Detailed examination of each of the remaining events in figure 15 reveals that substantially the same underlying mechanisms as illustrated in figures 19–22, are at work in each of these cases. In particular, the presence of a relatively strong vortex or counter-rotating pair of vortices ejects fluid from near the wall as it convects in the

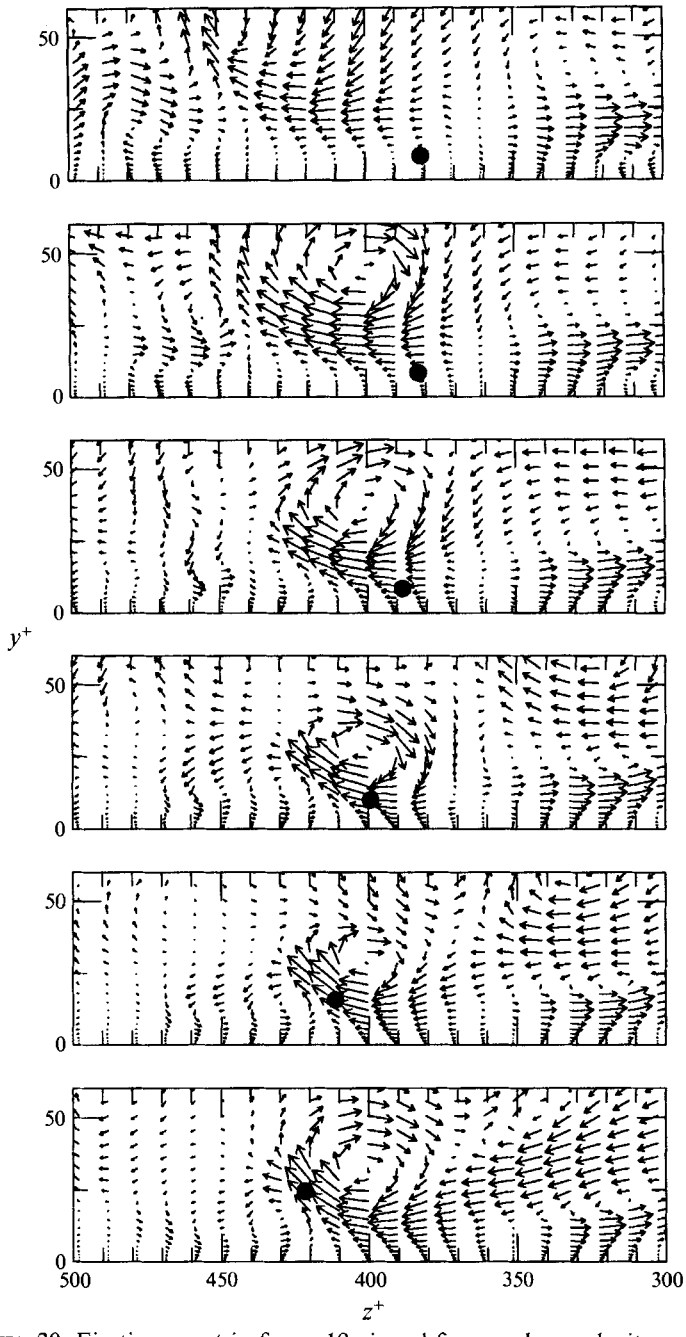

FIGURE 20. Ejection event in figure 19 viewed from end-on velocity vector plot.

flow. It is interesting to note that the velocity signals at fixed points in the vicinity of these events display a sharp rise in streamwise velocity reminiscent of the burst process (Bogard & Tiederman 1986). The present study thus supports the conclusion of Robinson (1991*a*) to the effect that bursts are due to the passage of quasi-streamwise vortices, rather than localized temporally intermittent eruptions of fluid away from the wall.

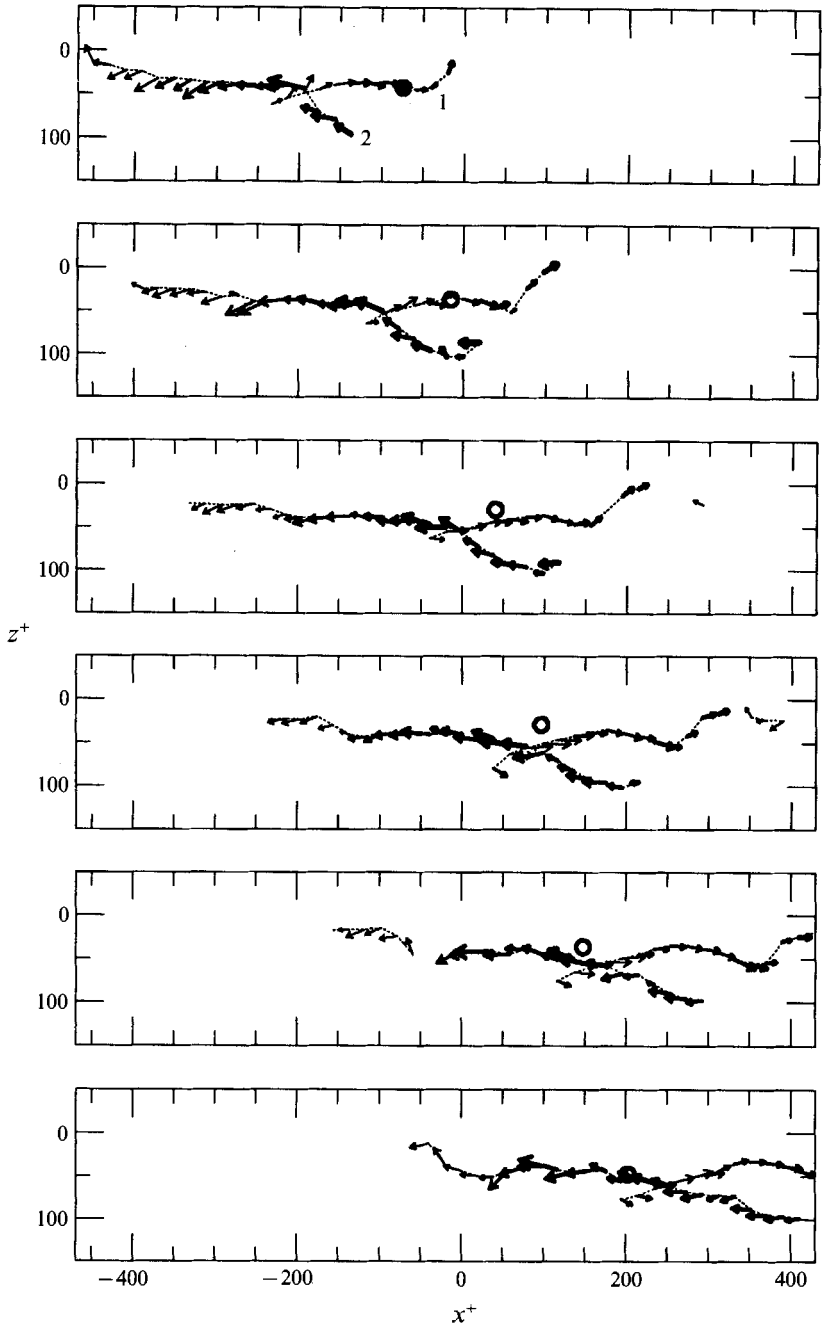

FIGURE 21. Time evolution of ejection event in plan view ending at $y^+ = 24.6$. Time increases in increments of $\Delta t^+ = 6.4$ from $t^+ = 0$ in the top figure until $t^+ = 32$ in the bottom figure.

Finally, we consider the relationship between vortical structures and the acceleration transport mechanism. A previous analysis of accelerating particle paths contributing to Reynolds stress (Handler *et al.* 1992) suggested a model for acceleration transport in which fluid particles experience a substantial change in streamwise velocity as they are propelled around the cores of quasi-streamwise vortices. In effect, the tilted vortices enhance the streamwise velocity field on one side and diminish it on the other so that

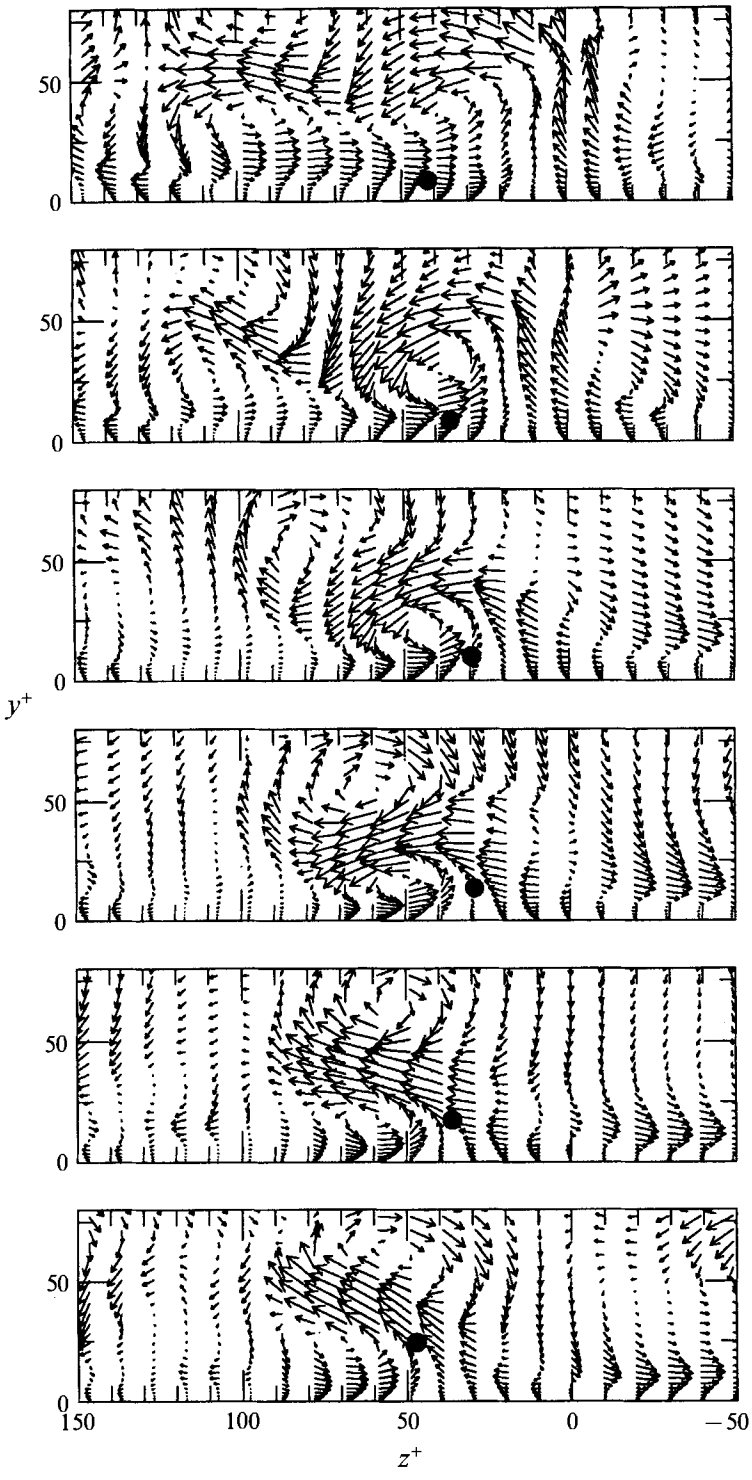

FIGURE 22. Ejection event in figure 21 viewed from end-on velocity vector plot.

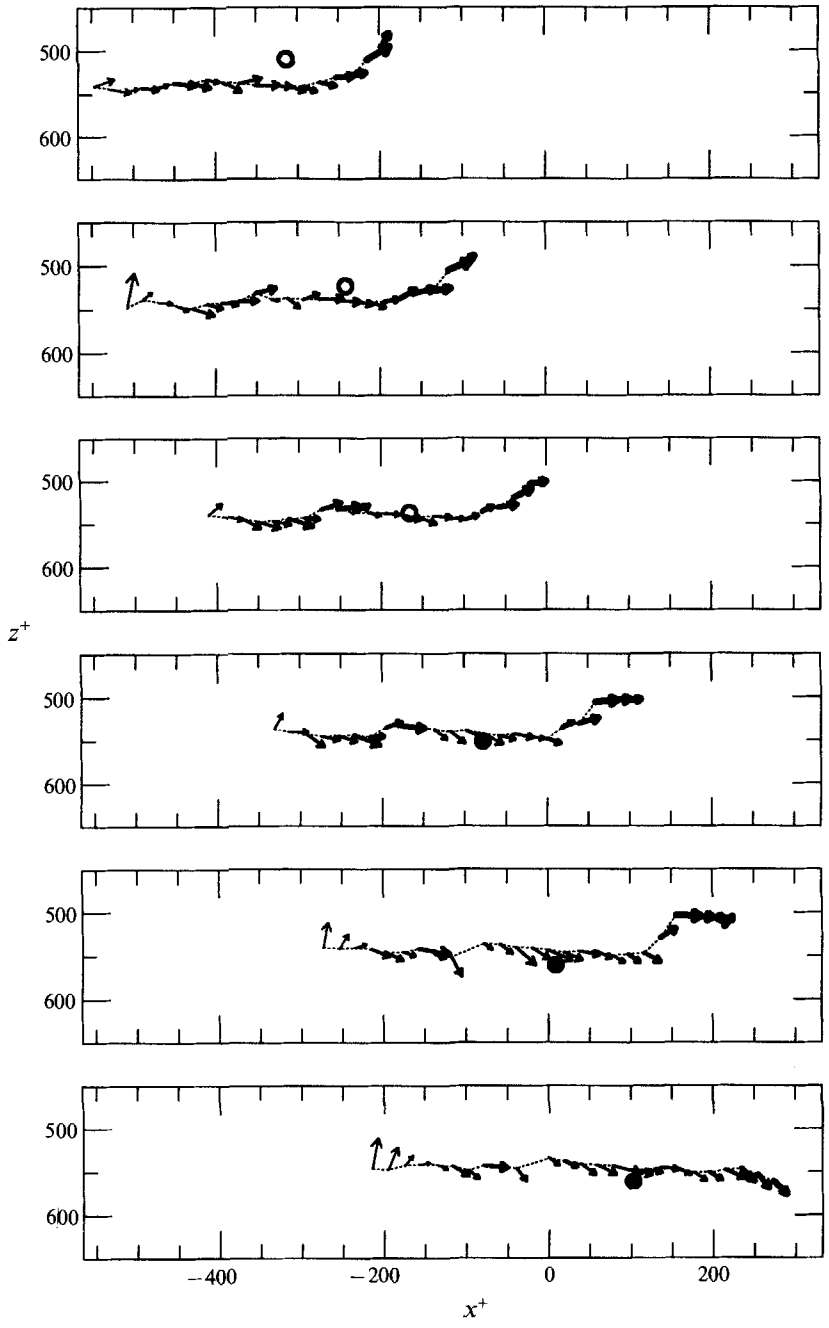

FIGURE 23. Time evolution of acceleration event in plan view ending at $y^+ = 24.6$. Time increases in increments of $\Delta t^+ = 6.4$ from $t^+ = 0$ in the top figure until $t^+ = 32$ in the bottom figure.

fluid particles accelerate as they travel from one side to the other. A particle turned away from the wall by the vortex decelerates while those turned towards it accelerate. In either case the signs of v_a and $U_a - U_b$ appearing in the last term in (2), are opposite.

This model is substantially confirmed by careful examination of each of the acceleration events shown in figure 16. A representative illustration of this process is given in figures 23 and 24 which refer to the event at $x^+ = 100, z^+ = 550$. The view in

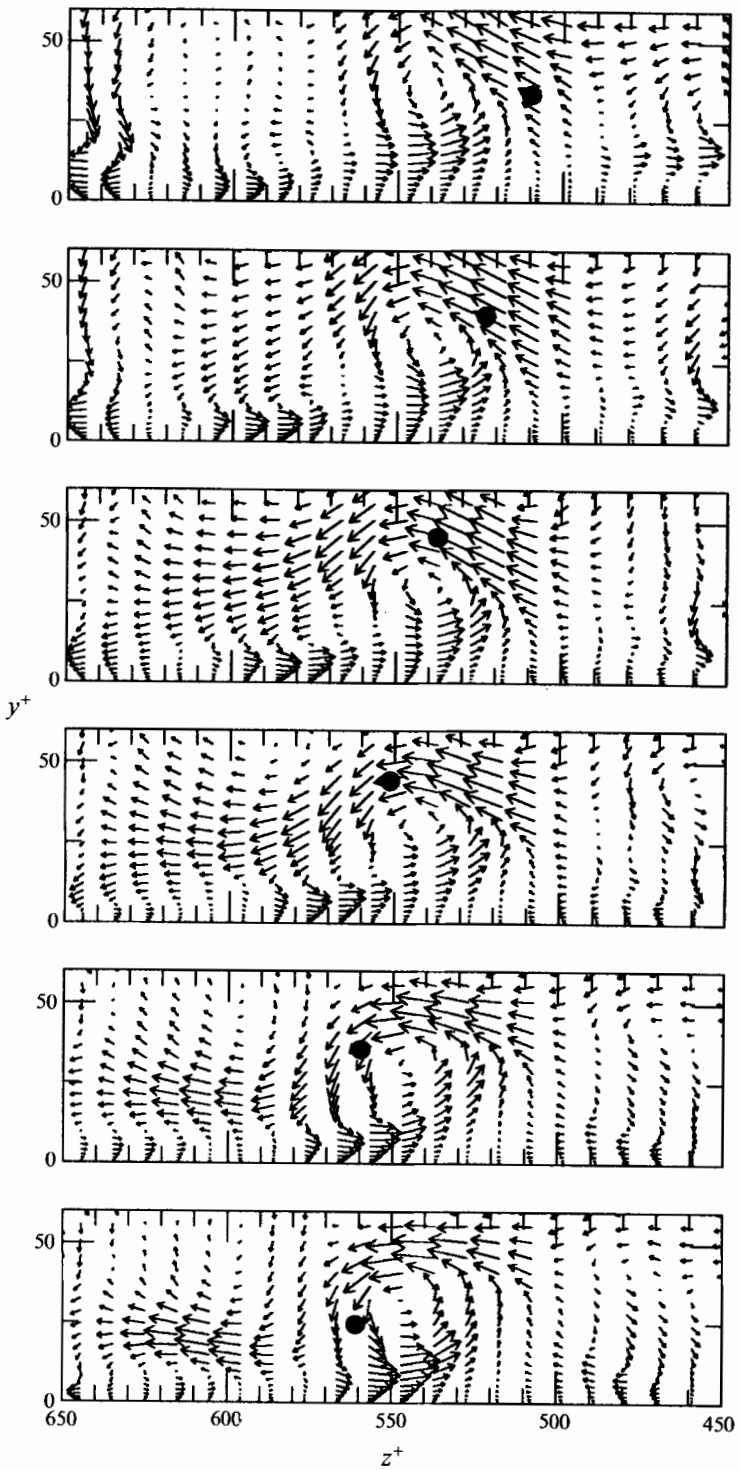

FIGURE 24. Acceleration event in figure 23 viewed from end-on velocity vector plot.

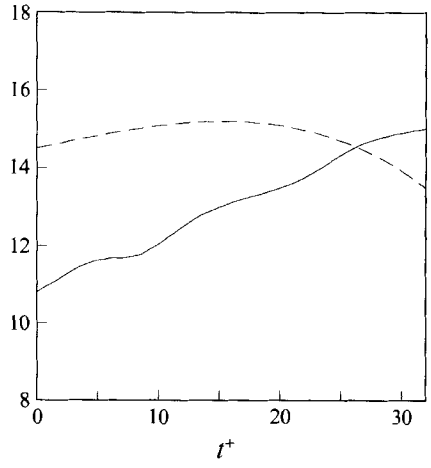

FIGURE 25. ——, Velocity of accelerating fluid particle; – – –, mean velocity at fluid particle location.

figure 23 is limited to a single vortex having a direct bearing on the event, together with one of the fluid particles. The contribution to acceleration transport by this particle is 44 times the average. As is clear from figure 24, the fluid particle travels around the core of the vortex. According to the model proposed by Handler *et al.* (1992), the fluid particle should experience a large streamwise acceleration even though it does not significantly change its altitude with respect to the wall. Figure 25 contains a plot of the particles' streamwise velocity together with the mean velocity corresponding to its altitude at any given time. Clearly, a very substantial streamwise acceleration – which is unrelated to a change in y^+ position – occurs as the particle negotiates around the vortex core. Examination of the other events in figure 16 yields many more examples of these findings. Consequently, acceleration transport appears to be an additional mechanism, besides the displacing of fluid particles, by which quasi-streamwise vortices generate significant amount of Reynolds stress in the near wall region.

6. Conclusions

The vortical events reconstructed in our simulation are sufficiently repetitive to suggest a complete scenario by which vortices evolve in the turbulent boundary layer. In agreement with a growing body of research, quasi-streamwise vortices are found to be the basic vortical element of the wall region. They have a pronounced capacity for self-replication leading to a continual supply of new structures. Evidently, turbulence is maintained in the flow since out of the many quasi-streamwise vortices produced, some manage to grow in size and strength to the point where they induce new quasi-streamwise vortices.

Vortices are created at the wall when pre-existing structures bring sufficiently strong rotation to points close enough to the boundary. The majority of new vortices form on the sweep side of structures but not exclusively so, as was documented in figures 9 and 10. The creation mechanism results in the common occurrence of nested vortices with the uplifted downstream parts of mature vortices convecting over newer vortices lying close to the wall.

Structures created near the wall migrate outwards while undergoing a dynamically changing array of interactions with other vortices. There is a considerable tendency for vortices in the outer flow to be kinked and sheared out of the streamwise direction,

which may partially explain why arch-like structures develop in the region away from the solid boundary. Convection of vortices at differing speeds enhances the opportunity for individual structures to dynamically encounter other nearby structures. Vortices with opposite streamwise rotation frequently interact, in whole or in part, in intensifying counter-rotating pairs thus aiding in the ejection and inrush of fluid particles. Wall pressure maxima are found to strongly reflect the presence of near-wall vortices, since they develop and convect in unison with the sweep side of such structures.

Analysis of the principal Reynolds stress events depicted in figures 14–16 permits the conclusion to be drawn that Reynolds stress production is inseparable from the dynamics of quasi-streamwise vortical structures in the wall region. The convection of individual and groups of structures along the wall leads to continuous ejections and sweeps contributing to displacement transport. The dominance of sweeps in producing Reynolds stress very close to the wall appears to be tied to the creation of new vortices at the surface. Tilted vortex cores accelerate fluid particles travelling to the wall and decelerate fluid particles leaving the wall region, thereby providing a mechanism for additional Reynolds stress production.

Finally, the vortical nature of Reynolds-stress-producing motions suggests an additional interpretation of the mixing time, as that interval over which vortices are able to exert control over the motion of individual fluid particles. During this time the correlation between u and v is created by the displacement and acceleration mechanisms induced by the vortices. The continual replaying of these transport inducing motions by each new generation of vortices maintains the Reynolds stress.

This work was supported through ONR contract N00014-91-WX-24079 and NRL grant 42-2010-91. Computer time was supplied by the Pittsburgh Supercomputing Center.

REFERENCES

AUBRY, N., HOLMES, P., LUMLEY, J. L. & STONE, E. 1988 The dynamics of coherent structures in the wall region of a turbulent boundary layer. *J. Fluid Mech.* **192**, 115–173.

AZAB, K. A. & MCLAUGHLIN, J. B. 1987 Modeling the viscous wall region. *Phys. Fluids* **30**, 2362–2373.

BAKEWELL, H. P. & LUMLEY, J. L. 1967 Viscous sublayer and adjacent wall region in turbulent pipe flow. *Phys. Fluids* **10**, 1880–1889.

BERNARD, P. S. & HANDLER, R. A. 1990*a* Reynolds stress and the physics of turbulent momentum transport. *J. Fluid Mech.* **220**, 99–124.

BERNARD, P. S. & HANDLER, R. A. 1990*b* On the dynamical significance of turbulent wall layer streaks. *Appl. Mech. Rev.* **43**, S219–S226.

BLACKWELDER, R. F., PANTON, R. L. & WALLACE, J. M. 1989 Questions from the Willmarth workshop on new directions in research on turbulent wall-layer structures. In *Some Unanswered Questions in Fluid Mechanics* (ed. L. M. Trefethen & R. L. Panton), *ASME Paper* 90-WA/FE-5, 28–32.

BOGARD, D. G. & TIEDERMAN, W. G. 1986 Burst detection with single-point velocity measurements. *J. Fluid Mech.* **162**, 389–413.

BROOKE, J. W. & HANRATTY, T. J. 1993 Origin of turbulence-producing eddies in a channel flow. *Phys. Fluids* A **5**, 1011–1022.

CHORIN, A. J. 1980 Vortex models and boundary layer instability. *SIAM J. Sci. Stat. Comput.* **1**, 1–21.

CHORIN, A. J. 1982 The evolution of a turbulent vortex. *Commun. Math. Phys.* **83**, 517–535.

ERSOY, S. & WALKER, J. D. A. 1986 The boundary layer due to a three-dimensional vortex loop. *AIAA J.* **24**, 1597–1605.

GRASS, A. J. 1971 Structural features of turbulent flow over smooth and rough boundaries. *J. Fluid Mech.* **50**, 233–255.

HANDLER, R. A., BERNARD, P. S., ROVELSTAD, A. L. & SWEARINGEN,, J. 1992 On the role of accelerating particles in the generation of Reynolds stress. *Phys. Fluids* A **4**, 1317–1319.

HANDLER, R. A., HENDRICKS, E. W. & LEIGHTON, R. I. 1989 Low Reynolds number calculation of turbulent channel flow: a general discussion. *Naval Res. Lab. Mem. Rep.* 6410.

HANRATTY, T. J. 1989 A conceptual model of the viscous wall region. In *Near Wall Turbulence Proc. Zaric. Meml. Conf.* (ed. S. J. Kline & N. H. Afgan), pp. 81–103. Hemisphere.

HERZOG, S. 1986 The large-scale structure in the near-wall region of turbulent pipe flow. PhD thesis, Cornell University.

HINZE, J. O. 1975 *Turbulence.* McGraw-Hill.

JANG, P. S., BENNEY, D. J. & GRAN, R. L. 1986 On the origin of streamwise vortices in a turbulent boundary layer. *J. Fluid Mech.* **169**, 109–123.

JIMENEZ, J. & MOIN, P. 1991 The minimal flow unit in near-wall turbulence. *J. Fluid Mech.* **225**, 213–240.

KASAGI, N., HIRATA, M. & NISHINO, K. 1986 Streamwise pseudo-vortical structures and associated vorticity in the near-wall region of a wall-bounded turbulent shear flow. *Exp. Fluids* **4**, 309–318.

KIM, H. T., KLINE, S. J. & REYNOLDS, W. C. 1971 The production of turbulence near a smooth wall in a turbulent boundary layer. *J. Fluid Mech.* **50**, 133–160.

KIM, J. 1987 Evolution of a vortical structure associated with the bursting event in a channel flow. *Turbulent Shear Flows 5* (ed. F. Durst, B. E. Launder, J. L. Lumley, F. W. Schmidt & J. H. Whitelaw), pp. 221–233. Springer.

KIM, J. 1989 On the structure of pressure fluctuations in simulated turbulent channel flow. *J. Fluid Mech.* **205**, 421–451.

KLINE, S. & ROBINSON, S. K. 1989 Turbulent boundary layer structure: progress, status and challenges. *Proc. 2nd IUTAM Symp. on Structure of Turbulence and Drag Reduction.* Fed. Inst. Tech., Zurich, Switzerland.

LIN, W.-Q. & BRASSEUR, J. G. 1990 Kinematics and dynamics of intermittent regions in homogeneous turbulent shear flow. *Bull. Am. Phys. Soc.* **35**, 2268.

LYONS, S. L., HANRATTY, T. J. & MCLAUGHLIN, J. B. 1989 Turbulence-producing eddies in the viscous wall region. *AIChE J.* **35**, 1962–1974.

MARCUS, P. S. 1984 Simulation of Taylor–Couette flow. Part 1. Numerical methods and comparison with experiment. *J. Fluid Mech.* **146**, 45–64.

MOIN, P. 1987 Analysis of turbulence data generated by numerical simulations. AIAA Paper 87-0194.

MOIN, P. & KIM, J. 1985 The structure of the vorticity field in turbulent channel flow. Part I. Analysis of instantaneous fields and statistical correlations. *J. Fluid Mech.* **155**, 441–464.

PEARSON, C. F. & ABERNATHY, F. H. 1984 Evolution of the flow field associated with a streamwise diffusing vortex. *J. Fluid Mech.* **146**, 271–284.

ROBINSON, S. K. 1991*a* The kinematics of turbulent boundary layer structure. *NASA Tech. Mem.* 103859.

ROBINSON, S. K. 1991*b* Coherent motions in the turbulent boundary layer. *Ann. Rev. Fluid Mech.* **23**, 601–639.

SMITH, C. R. & SCHWARTZ, S. P. 1983 Observations of streamwise rotation in the near-wall region of a turbulent boundary layer. *Phys. Fluids* **26**, 241–252.

SPALART, P. R. 1988 Direct simulation of a turbulent boundary layer up to $Re_\theta = 1410$. *J. Fluid Mech.* **187**, 61–98.

STRETCH, D., KIM, J. & BRITTER, R. 1990 A conceptual model for the structure of turbulent channel flow. *Proc. NASA Boundary-Layer Structure Workshop*, Hampton, VA.

WALLACE, J. M., ECKELMANN, H. & BRODKEY, R. S. 1972 The wall region in turbulent shear flow. *J. Fluid Mech.* **54**, 39–48.